

# On Detecting Biospheres from Chemical Thermodynamic Disequilibrium in Planetary Atmospheres

Joshua Krissansen-Totton,<sup>1</sup> David S. Bergsman,<sup>2</sup> and David C. Catling<sup>1</sup>

## Abstract

Atmospheric chemical disequilibrium has been proposed as a method for detecting extraterrestrial biospheres from exoplanet observations. Chemical disequilibrium is potentially a generalized biosignature since it makes no assumptions about particular biogenic gases or metabolisms. Here, we present the first rigorous calculations of the thermodynamic chemical disequilibrium in Solar System atmospheres, in which we quantify the available Gibbs energy: the Gibbs free energy of an observed atmosphere minus that of atmospheric gases reacted to equilibrium. The purely gas phase disequilibrium in Earth's atmosphere is mostly attributable to O<sub>2</sub> and CH<sub>4</sub>. The available Gibbs energy is not unusual compared to other Solar System atmospheres and smaller than that of Mars. However, Earth's fluid envelope contains an ocean, allowing gases to react with water and requiring a multiphase calculation with aqueous species. The disequilibrium in Earth's atmosphere-ocean system (in joules per mole of atmosphere) ranges from ~20 to 2 × 10<sup>6</sup> times larger than the disequilibria of other atmospheres in the Solar System, where Mars is second to Earth. Only on Earth is the chemical disequilibrium energy comparable to the thermal energy per mole of atmosphere (excluding comparison to Titan with lakes, where quantification is precluded because the mean lake composition is unknown). Earth's disequilibrium is biogenic, mainly caused by the coexistence of N<sub>2</sub>, O<sub>2</sub>, and liquid water instead of more stable nitrate. In comparison, the O<sub>2</sub>-CH<sub>4</sub> disequilibrium is minor, although kinetics requires a large CH<sub>4</sub> flux into the atmosphere. We identify abiotic processes that cause disequilibrium in the other atmospheres. Our metric requires minimal assumptions and could potentially be calculated from observations of exoplanet atmospheres. However, further work is needed to establish whether thermodynamic disequilibrium is a practical exoplanet biosignature, requiring an assessment of false positives, noisy observations, and other detection challenges. Our Matlab code and databases for these calculations are available, open source. Key Words: Biosignatures—Disequilibrium—Planetary atmospheres—Gibbs free energy—Exoplanets—Equilibrium—Thermodynamics. *Astrobiology* 16, 39–67.

## 1. Introduction

THE MOST INTERESTING question about exoplanets is whether any of them host life. In recent years, significant progress has been made in the detection and characterization of the atmospheres of Jupiter- and Neptune-sized exoplanets (Charbonneau *et al.*, 2002; Vidal-Madjar *et al.*, 2003; Barman, 2007; Pont *et al.*, 2008; Deming *et al.*, 2013; Fraine *et al.*, 2014). With the upcoming launch of NASA's James Webb Space Telescope and the construction of larger ground-based telescopes such as the European Extremely Large Telescope, it may be possible to constrain the atmospheric composition of terrestrial planets in the near future (Deming *et al.*, 2009; Belu *et al.*, 2011; Rauer *et al.*, 2011; Hedelt *et al.*, 2013; Snellen *et al.*, 2013; Misra *et al.*, 2014; Rodler and

López-Morales, 2014). Whether the presence of an exoplanet biosphere could be inferred remotely from these atmospheric observations needs to be carefully considered.

Life detection using remote sensing was first proposed in the 1960s and 1970s in the context of Solar System exploration (Lederberg, 1965). The realization that life on Earth has profoundly influenced the geochemical environment and, in particular, the composition of the atmosphere and oceans led naturally to the suggestion that alien biospheres may be detectable remotely via their influence on atmospheric composition (Lovelock, 1965, 1975; Lovelock and Margulis, 1974). More specifically, chemical disequilibrium in planetary atmospheres, such as the coexistence of two long-term incompatible species like oxygen and methane, was proposed as a possible sign of life (Lovelock, 1965;

<sup>1</sup>Department of Earth and Space Sciences/Astrobiology Program, University of Washington, Seattle, Washington.

<sup>2</sup>Department of Chemical Engineering, Stanford University, Stanford, California.

Hitchcock and Lovelock, 1967). It is now understood that all the bulk gases except for the inert gases in Earth's atmosphere are modulated by biology (Catling and Kasting, 2007), so it is reasonable to expect exoplanet atmospheres to be similarly perturbed away from chemical equilibrium by biogenic gas fluxes.

Chemical disequilibrium as a biosignature is appealing because unlike searching for biogenic gases specific to particular metabolisms, the chemical disequilibrium approach makes no assumptions about the underlying biochemistry. Instead, it is a generalized life-detection metric that rests only on the assumption that distinct metabolisms in a biosphere will produce waste gases that, with sufficient fluxes, will alter atmospheric composition and result in disequilibrium.

In the modern literature on exoplanets and astrobiology, atmospheric chemical disequilibrium is often cited as a possible means of life detection (Sagan *et al.*, 1993; Léger, 2000; Cockell *et al.*, 2009; Kasting *et al.*, 2009; Seager and Deming, 2010; Seager, 2014; Seager and Bains, 2015) and sometimes criticized (Schwartzman and Volk, 2004; Seager and Bains, 2015). However, this idea is not quantified, except in rare and specific instances. For example, Simoncini *et al.* (2013) used kinetic arguments and non-equilibrium thermodynamics to infer the minimum power that drives atmospheric disequilibrium for Earth and Mars, and Seager *et al.* (2013) applied kinetic arguments to deduce biomass estimates for biosignature gas detections. Kleidon (2012) reviewed the mechanisms for free energy generation on Earth and the possible effects of increasing human consumption of free energy, while Ulanowicz and Hannon (1987) argued that surfaces dominated by biology such as tropical rainforests are more dissipative than desert surfaces, and that this difference in entropy production might be accessible to remote sensing. Estrada (2012) introduced a novel but perhaps non-intuitive atmospheric disequilibrium metric based on examining the directionality of the network of chemical reactions in an atmosphere. Estrada's method highlights species injected into an atmosphere, but many of them for Earth are anthropogenic, such as halocarbons.

*Thermodynamic* disequilibrium in planetary atmospheres and its quantification for biosignature detection on exoplanets has not been examined for several decades. Lippincott *et al.* (1967) and Lovelock (1975) made early attempts to calculate thermodynamic disequilibrium for the Solar System planets, but knowledge of the actual atmospheric composition of Solar System planets, computational methods, and thermodynamic data for chemical equilibrium calculations have since greatly improved. Additionally, Lovelock (1975), who is the only author to report the magnitude of disequilibrium in Earth's atmosphere-ocean system, did not provide the details of his method. However, we infer that he probably used analytic calculations and assumed that key redox couples reacted to completion (see the results section). This method does not give the correct answer for the thermodynamic equilibrium of the Earth atmosphere-ocean system because completion is not necessarily the same as the equilibrium state.

Another important issue is that all atmospheres are in disequilibrium to some extent because they receive a free energy flux from sunlight and, more generally, could obtain additional free energy from release of volcanic gases, tidal

energy, or internal heat. Indeed, there are already ostensible detections of thermodynamic disequilibrium in the atmospheres of transiting, jovian-like exoplanets [*e.g.*, Knutson *et al.* (2012); Moses *et al.* (2011); Stevenson *et al.* (2010), although see Line and Yung (2013) for an alternative view]. Consequently, inferring life from atmospheric thermodynamic disequilibrium is a question of degree. To understand the issue properly, accurate quantification is necessary. Thus, part of the purpose in this work is to examine the abiotic disequilibria in Solar System atmospheres and compare the results with Earth.

Here, we present a rigorous methodology and calculation of thermodynamic disequilibrium in the atmospheres of Solar System planets and Saturn's largest moon, Titan, using Gibbs free energy. We quantify chemical disequilibrium in atmospheres as the difference between the Gibbs energy of observed atmospheric constituents and the Gibbs free energy of the same atmosphere if all its constituents were reacted to equilibrium under prevailing conditions of temperature and pressure. For Earth, the purely gas phase calculation does not capture the disequilibrium in the atmosphere-ocean system, so we present a method for quantifying the atmosphere-ocean disequilibrium using multiphase Gibbs energy minimization. We do not consider kinetic disequilibrium in our analysis, which will be the topic of future work. Finally, we discuss whether using thermodynamic disequilibrium as a biosignature is feasible on both practical and theoretical grounds. To promote cooperation in research, our Matlab source code and all the databases used for these calculations are available as postpublication open source software.

## 2. Methods

### 2.1. Gas phase calculations

Appendix A gives specifics on the gas phase calculations, and here we outline the general methodology. To quantify thermodynamic disequilibrium, we model each atmosphere as a well-mixed closed system at a constant pressure (surface pressure or 1 bar for giant planets) and temperature (global mean surface temperature or the mean temperature at the 1 bar level for giant planets). Thermodynamic theory states that, for a closed chemical system at constant temperature and pressure, chemical equilibrium is achieved when the Gibbs free energy of the system is minimized.

If there are  $N$  chemical species in an atmosphere containing  $n_i$  moles of each gas  $i$ , then the total Gibbs free energy of the system (in joules) is

$$\begin{aligned} G_{(T,P)} &= \sum_i^N \left( \frac{\partial G}{\partial n_i} \right)_{T,P} n_i = \sum_i^N \mu_i n_i \\ &= \sum_i^N \left( \mu_i - G_{i(T,P_r)}^\circ + G_{i(T,P_r)}^\circ \right) n_i \end{aligned} \quad (1)$$

Here,  $\mu_i$  (J/mol) is the partial molar Gibbs free energy, or equivalently, the chemical potential (see Anderson, 2005),  $G_{i(T,P_r)}^\circ$  is the standard partial molar Gibbs free energy of gas  $i$  at reference pressure  $P_r$ , which is typically 1 bar or 1 atm depending on the database used. We have written the expression in the second line of Eq. 1 because a basic relationship in thermodynamics (the definition of chemical potential) is

$$\mu_i - G_{i(T,P_r)}^\circ = RT \ln(a_i) = RT \ln\left(\frac{f_i}{f_i^\circ}\right) = RT \ln\left(\frac{P_i \gamma_{fi}}{P_r \gamma_{fi}^\circ}\right) \quad (2)$$

Here,  $a_i = f_i/f_i^\circ$  is the activity of species  $i$ ,  $f_i$  denotes partial fugacity,  $f_i^\circ$  is a reference partial fugacity,  $\gamma_{fi}$  is the activity coefficient of species  $i$ , with  $\gamma_{fi}^\circ$  a standard value, and  $P_i$  is partial pressure of species  $i$ . See the work of Anderson (2005, pp 198–208) for a derivation of Eq. 2. The activities of reacting species are given by

$$a_i = \left(\frac{f_i}{f_i^\circ}\right) = P_i \gamma_{fi} = \frac{P n_i}{n_T} \gamma_{fi} \quad (3)$$

where we have taken  $f_i^\circ = 1$  bar as the reference state,  $n_i$  is the number of moles of species  $i$ ,  $n_T$  is the total number of moles, and  $P = \sum_i P_i$  is the total pressure by Dalton's law.

Substitution of Eqs. 2 and 3 into Eq. 1 gives the following expression for the Gibbs free energy of an atmosphere, where we drop the “ $N$ ” in the summation to avoid clutter:

$$\begin{aligned} G_{(T,P)} &= \sum_i n_i (G_{i(T,P_r)}^\circ + RT \ln(a_i)) \\ &= \sum_i n_i (G_{i(T,P_r)}^\circ + RT \ln(P n_i \gamma_{fi} / n_T)) \end{aligned} \quad (4)$$

This is a form of Gibbs free energy used in previous Gibbs free energy minimization schemes minimum (White *et al.*, 1958; Eriksson, 1971, 1975; Venot *et al.*, 2013). Here,  $G_{(T,P)}$  is the Gibbs free energy of the system at constant temperature,  $T$ , and constant pressure,  $P$ . The number of moles of the  $i^{\text{th}}$  atmospheric species is given by  $n_i$ , the standard Gibbs free energy of the  $i^{\text{th}}$  species at some reference pressure  $P_r$  is given by  $G_{i(T,P_r)}^\circ$ , and  $R = 8.314$  J/mol is the universal gas constant. Variables  $\gamma_{fi}$  and  $n_T$  were defined earlier. The summation in Eq. 4 is over all molecular species in the planet's atmosphere. For purely gas phase calculations, we will take  $n_T = 1$  so that mixing ratios can be substituted for  $n_i$  and all Gibbs energy results will be in units of joules per mole of atmosphere. For example, for Earth,  $n_{O_2} \approx 0.21$  and  $n_{N_2} \approx 0.78$ .

In practice, Gibbs free energy is only defined relative to some reference energy, so we substitute absolute Gibbs energies for Gibbs energies of formation to obtain

$$\begin{aligned} \Delta G_{(T,P)} &= \sum_i n_i (\Delta_f G_{i(T,P_r)}^\circ + RT \ln(P_i \gamma_{fi})) \\ &= \sum_i n_i (\Delta_f G_{i(T,P_r)}^\circ + RT \ln(P n_i \gamma_{fi} / n_T)) \end{aligned} \quad (5)$$

Here,  $\Delta_f G_{i(T,P_r)}^\circ$  is the standard free energy of formation for the  $i^{\text{th}}$  species. This is defined as the free energy change associated with forming the  $i^{\text{th}}$  species from its constituent elements at temperature  $T$  and pressure  $P_r$ . It can be shown that the minimum of Eq. 4 is identical to the minimum of Eq. 5 (see Appendix B for this proof), so in practice we find the equilibrium state by finding the equilibrium  $n_i$  that minimizes Eq. 5, which we represent with an overbar as  $\bar{n}_i$ .

Temperature-dependent standard Gibbs free energies of formation were calculated from enthalpies and entropies of formation retrieved from NASA's thermodynamic database (Burcat and Ruscic, 2005). Some atmospheres such as that of Venus have high surface temperature and pressure, so

their constituent gases exhibit non-ideal behavior. We account for this by calculating temperature and pressure-dependent fugacity coefficients for each species using the Soave equation as described in Walas (1985, p 146). The Soave equation is an empirical equation of state that accounts for the nonzero volume of particles and attractive forces between pairs of particles. To calculate fugacity coefficients for a known mixture of gases at a specified temperature and pressure, the critical temperatures, critical pressures, acentric factors (a measure of non-sphericity of molecules), and binary interaction parameters for all the constituent species are required. We obtained critical temperatures, critical pressures, and acentric factors from the work of Perry and Green (2008, Section 2-136). Tests indicate that binary interaction parameters have a negligible effect on the overall Gibbs energy changes we are interested in, so all binary interaction parameters were assumed to be zero in our analysis (see Appendix A). Because the fugacity coefficient is a function of species concentration, the fugacity coefficients of all gaseous species were recalculated at every iteration in our optimization routine to ensure convergence to the correct equilibrium. Typically, including fugacity coefficients does not change the results very much for Earth-like temperatures and pressures. However, for high-pressure atmospheres such as Venus, fugacity coefficients are important because the departures from ideal gas behavior are appreciable.

For any observed planetary atmosphere with a composition specified by mole fractions  $n_i$ , the equilibrium composition can be found by determining the mole fractions  $\bar{n}_i$  that minimize  $\Delta G_{(T,P)}$  in Eq. 5 subject to the constraint that atoms are conserved. The atom constraint condition is given by

$$\begin{aligned} \text{Equilibrium moles of element } k &= \text{Observed moles of element } k \\ \sum_i \nu_{ki} \bar{n}_i &= \sum_i \nu_{ki} n_i \end{aligned} \quad (6)$$

Here,  $\nu_{ki}$  is the number of atoms of element  $k$  per molecule of the  $i^{\text{th}}$  species.

The above framework is a constrained, nonlinear optimization problem: the equilibrium state of an atmosphere can be found by minimizing Eq. 5 subject to Eq. 6. We used an interior points method (Byrd *et al.*, 1999, 2000) implemented by using Matlab's *fmincon* function to solve this optimization problem. Interior points is an efficient and reliable optimization technique known to be useful for chemical equilibrium problems (see Karpov *et al.*, 1997, and references therein). For gas phase Gibbs energy minimization, the equation to be optimized is convex (has non-negative second derivative), so any local minimum will be the single global minimum (White *et al.*, 1958).

To quantify the chemical disequilibrium in a planet's atmosphere, we define the “available Gibbs energy,”  $\Phi$ , as the difference in Gibbs free energy between the observed (initial) state and the equilibrium state:

$$\Phi \equiv G_{(T,P)}(n_i) - G_{(T,P)}(\bar{n}_i) \quad (7)$$

Since Gibbs free energy is only defined relative to some reference energy, in practice we compute available Gibbs energy using this equivalent expression:

$$\Phi = \Delta G_{(T,P)}(n_i) - \Delta G_{(T,P)}(\bar{n}_i) \quad (8)$$

See Appendix B for a proof of the equivalence of Eqs. 7 and 8. The available Gibbs energy,  $\Phi$ , has units of joules per mole of atmosphere. Thermodynamic theory states that this Gibbs free energy difference is the maximum useful work that can be extracted from the system. In other words,  $\Phi$  is the untapped chemical free energy in a planet's atmosphere and so provides our metric of disequilibrium.

## 2.2. Multiphase calculations

The numerical approach described above applies to gaseous systems only such as Mars, Venus, and Jupiter. To calculate chemical disequilibrium for planets with surface oceans, we reformulate the Gibbs energy expression for multiphase systems. Appendix C gives specifics of the multiphase calculations, and here we provide a general overview. We follow Karpov *et al.* (1997) and use the following expression for the Gibbs energy of a multiphase system:

$$\Delta G_{(T,P)} = \sum_i c_i n_i + \sum_{\alpha} \sum_{i \in \alpha} n_i RT \ln(n_i/n_{\alpha}) - \sum_{j=\text{aqueous species}} n_j RT \ln(n_w/n_{aq})$$

$$c_i = \begin{cases} \Delta_f G_{i(T,P)}^{\circ} + RT \ln(\gamma_{fi}) + RT \ln(P), & i \in \text{gas} \\ \Delta_f G_{i(T,P)}^{\circ} + RT \ln(\gamma_{aw}), & i \in \text{water} \\ \Delta_f G_{i(T,P)}^{\circ} + RT \ln(\gamma_{ai}) + RT \ln(55.5084), & i \in \text{aqueous} \end{cases} \quad (9)$$

Here, we have simplified equations of Karpov *et al.* (1997) to exclude solid phases and nonwater pure liquids because we do not consider such systems in this study. In addition to the variables already defined above, we have the following:

- $\alpha$  = index for the phase (gaseous, water, or aqueous)
- $n_{\alpha}$  = total number of moles of species in phase  $\alpha$
- $n_w$  = total number of moles of liquid water in the system
- $n_{aq}$  = total number of moles of aqueous species in the system
- $\gamma_{aw}$  = activity coefficient of water
- $\gamma_{ai}$  = activity coefficient of the  $i^{\text{th}}$  aqueous species

We see that Eq. 9 for the gas phase system ( $c_i, i \in \text{gas}$ ) is identical to Eq. 5 if we let  $n_{\alpha} = n_T$ .

To calculate the equilibrium state of Earth's atmosphere-ocean system, we minimize Eq. 9 above subject to the constraint that atoms and charge are conserved, where the latter means that aqueous systems are electroneutral. The atom constraint is identical to that used for the gaseous systems as defined by Eq. 6. The charge constraint is given by

*Total charge in equilibrium = Total charge in observed state*

$$\sum_i q_i \bar{n}_i = \sum_i q_i n_i \quad (10)$$

Here,  $q_i$  is the charge per molecule of the  $i^{\text{th}}$  species. Just as for the gaseous calculations, the Gibbs energy difference between the observed and equilibrium states,  $\Phi$ , can be calculated once the equilibrium state is determined.

Temperature and pressure-dependent Gibbs free energies of formation for aqueous species were calculated from the

SPRONS96 database in SUPCRT (Johnson *et al.*, 1992) and the methodology described by Walther (2009). We assumed that the Born coefficients, which describe species-specific solvation properties, would have a negligible effect on Gibbs energies, so those terms were dropped from the calculations. Activity coefficients for aqueous species were approximated using the Truesdell-Jones equation and thermodynamic coefficients from Langmuir (1997, p 133) (see Appendix C). For Earth, the available Gibbs energy is quite sensitive to water activity. Thus, rather than use the approximation above, the activity coefficient for water was calculated rigorously by using a simplified form of the Pitzer equations (Marion and Kargel, 2007) and Pitzer coefficients from the work of Apelo and Postma (2005) and Marion (2002).

Finding the equilibrium state for multiphase systems is more challenging than for single-phase gaseous systems. The Matlab function *fmincon* was once again used to implement the optimization, but this time we provided the analytic first derivative gradient for the Gibbs energy function in Eq. 9. This ensured more rapid and reliable convergence. For multiphase Gibbs energy minimization problems, there is no guarantee that the local minima equal the global minimum (Nichita *et al.*, 2002). Consequently, we implemented a simple global minimum search by iterating over a large ensemble of initial conditions and selecting the solution from the ensemble with the minimum of the minima (see Appendix C for details).

## 2.3. Semianalytic validation

Validation of gas phase calculations was initially done using a classic textbook case from the work of Balzhiser *et al.* (1972, pp 513–527), which was found to match our numerical calculations. This textbook case was a gas phase reaction of ethane and steam at 1000 K to form  $H_2$ , CO, and various hydrocarbons. We also correctly solved the equilibrium using the method of Lagrange multipliers as a check.

Furthermore, to corroborate the numerical Gibbs free energy calculations for planetary atmospheres, we also approximated the available Gibbs energy in each atmosphere using a simple analytic expression. For a single reaction between arbitrary reactants and products,



The Gibbs energy of this reaction is given by

$$\Delta_r G = \Delta_r G^{\circ} + RT \ln(Q) = \Delta_r G^{\circ} + RT \ln\left(\frac{a_{P_1}^C a_{P_2}^D}{a_{R_1}^A a_{R_2}^B}\right) \quad (12)$$

Here, A, B, C, and D are the stoichiometric coefficients representing reactants  $R_1$  and  $R_2$ , products  $P_1$  and  $P_2$ , respectively. The activity of each species is  $a_X$ ,  $R$  is the universal gas constant, and  $T$  is the temperature of the system. The left-hand side of Eq. 12,  $\Delta_r G$ , is the change in Gibbs energy of the system per A moles of reactant  $R_1$  and B moles of reactant  $R_2$  that are converted to products. The standard free energy of the reaction,  $\Delta_r G^{\circ}$ , represents the Gibbs energy of the reaction when the activities of all species equal unity. At equilibrium, the left-hand side of Eq. 12 equals zero. This equilibrium can be found by appropriate substitution for each of the activities in terms of initial

TABLE 1. EQUILIBRIUM CALCULATION FOR VENUS' ATMOSPHERE ( $T=735.3$  K,  $P=92.1$  BAR)

<i>Species</i>	<i>Initial mixing ratio</i>	<i>Final abundance (fmincon)</i>	<i>Final abundance (Aspen)</i>	<i>Final – initial abundance (fmincon)</i>
CO <sub>2</sub>	<b>0.965</b>	<b>0.965004</b>	<b>0.9650041</b>	<b>0.0000039</b>
N <sub>2</sub> *	0.034715	0.034715	0.034715	-6.21E-13
SO <sub>2</sub>	<b>0.00015</b>	<b>0.000148</b>	<b>0.000147949</b>	<b>-0.00000197</b>
H <sub>2</sub> O	<b>0.00003</b>	<b>3.00329E-05</b>	<b>3.00295E-05</b>	<b>3.29E-08</b>
Ar	0.000061	0.000061	0.000061	0
CO	<b>0.000017</b>	<b>1.07569E-05</b>	<b>1.04986E-05</b>	<b>-0.00000624</b>
He	0.000009	0.000009	0.000009	0
Ne	0.000007	0.000007	0.000007	0
OCS	<b>0.00001</b>	<b>1.23452E-05</b>	<b>1.24294E-05</b>	<b>0.00000235</b>
H <sub>2</sub> S	<b>0.00000007</b>	<b>4.00713E-08</b>	<b>4.13474E-08</b>	<b>-2.99E-08</b>
HCl	0.0000005	0.0000005	0.0000005	0
Kr	0.000000025	0.000000025	0.000000025	0
S	<b>0.00000035</b>	<b>1.34652E-10</b>	<b>2.1696E-17</b>	<b>-0.00000035</b>
HF	4.5E-09	4.5E-09	4.5E-09	0
Xe	0.00000002	0.00000002	0.00000002	0
H <sub>2</sub>	<b>0.000000003</b>	<b>7.5802E-11</b>	<b>2.13576E-09</b>	<b>-2.92E-09</b>
NH <sub>3</sub>	<b>1E-14</b>	<b>1.25215E-12</b>	<b>1.1679E-14</b>	<b>1.24E-12</b>

The second column gives the observed surface mixing ratios of all species in Venus' atmosphere, and the third column gives the equilibrium abundances of each species as determined by our own Gibbs free energy minimization Matlab code. The fourth column is an independent validation of the equilibrium abundances calculated using the commercial software package Aspen Plus. The fifth column gives the change in abundance for each species according to our Gibbs energy minimization (column three minus column two). Rows in boldface highlight the species where abundances change during the reaction to equilibrium. The available Gibbs energy from our own code is  $\Phi=0.0596$  J/mol.

\*N<sub>2</sub> was slightly modified from textbook value to ensure mixing ratios summed to 1.

abundances and the total moles reacted to reach equilibrium (the only unknown variable), and by solving the resultant polynomial (see Appendix D). This equilibrium condition is equivalent to minimizing the Gibbs energy of the same system by using Eq. 5.

The available Gibbs energy of the system,  $\Phi$ , can be obtained by integrating  $\Delta_r G$  from the initial state to the equilibrium state. Strictly speaking, this semianalytic approach can only be applied to systems of gases where there is only one possible reaction, and not to complex mixtures of gases such as planetary atmospheres. However, this calculation can be repeated for all the key reactions in a

planet's atmosphere, and the summed available Gibbs energies can be compared to the numerical result from Gibbs energy minimization. The key reactions for these semi-analytic calculations were chosen using the important redox couples identified by chemical intuition for each atmosphere. The two approaches are not exactly equivalent because treating each reaction independently does not account for interactions between multiple reactions. To simplify the semianalytic calculations, we also make the assumption that the total moles in the atmosphere remain unchanged as the reaction proceeds. Consequently, we expect small differences between the semianalytic and numerical approaches.

TABLE 2. EQUILIBRIUM CALCULATION FOR MARS' ATMOSPHERE ( $T=214$  K,  $P=0.006$  BAR)

<i>Species</i>	<i>Initial mixing ratio</i>	<i>Final abundance (fmincon)</i>	<i>Final abundance (Aspen)</i>	<i>Final – initial abundance (fmincon)</i>
CO <sub>2</sub>	<b>0.9597</b>	<b>0.960257</b>	<b>0.960257</b>	<b>0.000557</b>
N <sub>2</sub>	0.0189	0.0189	0.0189	5E-10
Ar*	0.019165	0.019165	0.0191646	0
O <sub>2</sub>	<b>0.00146</b>	<b>0.001175</b>	<b>0.00117462</b>	<b>-0.00028538</b>
CO	<b>0.000557</b>	<b>5.51991E-17</b>	<b>0</b>	<b>-0.000557</b>
H <sub>2</sub> O	<b>0.0002</b>	<b>0.000215</b>	<b>0.00021504</b>	<b>0.000015</b>
NO	<b>0.000000001</b>	<b>2.36011E-16</b>	<b>1.96E-24</b>	<b>-0.000000001</b>
Ne	0.0000025	0.0000025	0.0000025	0
Kr	0.0000003	0.0000003	0.0000003	0
Xe	0.00000008	0.00000008	0.00000008	0
O <sub>3</sub>	<b>0.0000004</b>	<b>8.702E-17</b>	<b>0</b>	<b>-0.0000004</b>
NO <sub>2</sub>	1E-30	8.84675E-16	6.19E-17	8.85E-16
H <sub>2</sub>	<b>0.000015</b>	<b>6.01993E-17</b>	<b>0</b>	<b>-0.000015</b>
H <sub>2</sub> O <sub>2</sub>	<b>0.00000004</b>	<b>1.19914E-16</b>	<b>0</b>	<b>-0.00000004</b>

Columns are the same as in Table 1. The initial mixing ratios are surface abundances. The available Gibbs energy from our own code is  $\Phi=136.3$  J/mol.

\*Ar was modified slightly from textbook value to ensure mixing ratios summed to 1.

TABLE 3. EQUILIBRIUM CALCULATION FOR JUPITER'S ATMOSPHERE

<i>Species</i>	<i>Initial mixing ratio</i>	<i>Final abundance (fmincon)</i>	<i>Final abundance (Aspen)</i>	<i>Final – initial abundance (fmincon)</i>
H <sub>2</sub>	<b>0.862</b>	<b>0.86199998</b>	<b>0.862</b>	<b>-1.56E-08</b>
He*	0.136024	0.136024	0.136024	0
CH <sub>4</sub>	<b>0.00181</b>	<b>0.001810005</b>	<b>0.00181001</b>	<b>5.2E-09</b>
NH <sub>3</sub>	<b>0.00013</b>	<b>0.000130004</b>	<b>0.000130004</b>	<b>3.6E-09</b>
Ne	0.0000199	0.0000199	0.0000199	0
Ar	0.0000157	0.0000157	0.0000157	0
H <sub>2</sub> O	<b>0.000000001</b>	<b>2.6E-09</b>	<b>2.6E-09</b>	<b>1.6E-09</b>
CO	<b>1.6E-09</b>	<b>1.13471E-19</b>	<b>0</b>	<b>-1.6E-09</b>
HCN	<b>3.6E-09</b>	<b>9.49988E-20</b>	<b>0</b>	<b>-3.6E-09</b>

Columns are the same as in Table 1. The initial mixing ratios are abundances at the 1 bar level ( $T=165\text{K}$ ). The available Gibbs energy from our own code is  $\Phi=0.00103\text{J/mol}$ .

\*He was modified from textbook value to ensure mixing ratios summed to 1.

Appendix D gives step-by-step detail on semianalytic procedures. The semianalytic approximations described above for gas phase systems can also be applied to aqueous reactions in a multiphase system such as Earth.

#### 2.4. Validation using Aspen Plus

Both gaseous and multiphase calculations were validated using the commercial software package Aspen Plus (Version 8.6), which is commonly used in chemical engineering. Aspen Plus provided a completely independent check of our calculations because it uses different thermodynamic databases and property models to both our Matlab calculations and semianalytic approximations. We used an equilibrium reactor called “RGIBBS” in Aspen Plus to implement gas phase and multiphase equilibrium calculations by Gibbs free energy minimization. We also used the Peng-Robinson equation of state (Prausnitz *et al.*, 1999) model for gas phase calculations, which is appropriate for the temperatures and

pressures we are interested in. For multiphase calculations, we used a “Flash2” phase separator in the Aspen Plus model in addition to an RGIBBS reactor, which ensured that the phases of aqueous species were correctly assigned. Without the phase separator, the equilibrium results were unphysical, and the resultant Gibbs energy change was inaccurate. We report results from the Electrolyte Non-Random Two Liquid (ELECNRTL) model in the main text (*e.g.*, see Prausnitz *et al.*, 1999, Chapter 6). ELECNRTL is the recommended activity coefficient model for calculations involving electrolytes (Aspen Technology Inc., 2000). Appendix E explains the Aspen Plus multiphase calculation in more detail and reports results for a different electrolyte model.

#### 2.5. Planetary data

The observed atmospheric compositions used in this analysis were obtained from a variety of up-to-date sources.

TABLE 4. Equilibrium Calculation for Titan's Atmosphere ( $T=93.65\text{K}$ ,  $P=1.46\text{BAR}$ )

<i>Species</i>	<i>Initial mixing ratio</i>	<i>Final abundance (fmincon)</i>	<i>Final abundance (Aspen)</i>	<i>Final – initial abundance (fmincon)</i>
N <sub>2</sub> *	0.94179679	0.94179679	0.9417968	0
CH <sub>4</sub>	<b>0.05712</b>	<b>0.057144</b>	<b>0.057144</b>	<b>0.000024</b>
H <sub>2</sub>	<b>0.00099</b>	<b>0.000974</b>	<b>0.000974</b>	<b>-0.000016</b>
CO	<b>0.000047</b>	<b>4.7E-05</b>	0.000047	-3.46E-19
Ar	0.00003421	0.00003421	0.0000342	0
C <sub>2</sub> H <sub>6</sub>	<b>0.00001</b>	<b>3.97606E-19</b>	<b>0</b>	<b>-0.00001</b>
C <sub>2</sub> H <sub>2</sub>	<b>0.000002</b>	<b>6.1423E-20</b>	<b>0</b>	<b>-0.000002</b>
HCN	1E-20	1.15092E-19	0	1.05E-19
C <sub>3</sub> H <sub>8</sub>	1E-20	1.9732E-19	0	1.87E-19
C <sub>2</sub> H <sub>4</sub>	1E-20	1.1886E-19	0	1.09E-19
CH <sub>3</sub> C <sub>2</sub> H	1E-20	5.65276E-20	NA	4.65E-20
C <sub>2</sub> N <sub>2</sub>	1E-20	4.97628E-20	0	3.98E-20
C <sub>3</sub> HN	1E-20	3.86518E-20	NA	2.87E-20
CH <sub>3</sub> CN	1E-20	1.11588E-19	NA	1.02E-19
C <sub>4</sub> H <sub>8</sub> _I	1E-20	8.17504E-20	NA	7.18E-20
C <sub>4</sub> H <sub>10</sub> _I	1E-20	1.38594E-19	NA	1.29E-19
C <sub>6</sub> H <sub>6</sub>	1E-20	2.69708E-20	0	1.7E-20
NO <sub>2</sub>	1E-20	1.18993E-19	0	1.09E-19
NO	1E-20	1.36611E-19	0	1.27E-19

Columns are the same as in Table 1. The initial mixing ratios are surface abundances. The available Gibbs energy from our own code is  $\Phi=1.21\text{J/mol}$ . NA indicates that these species were not included in the Aspen Plus calculation.

\*N<sub>2</sub> was modified from textbook value to ensure mixing ratios summed to 1.

TABLE 5A. EQUILIBRIUM CALCULATION FOR URANUS' ATMOSPHERE

<i>Species</i>	<i>Initial mixing ratio</i>	<i>Final abundance (fmincon)</i>	<i>Final abundance (Aspen)</i>	<i>Final – initial abundance (fmincon)</i>
H <sub>2</sub>	0.825	0.825	0.825	0
He*	0.1519987	0.1519987	0.1519987	0
CH <sub>4</sub>	0.023	0.023	0.023	0
NH <sub>3</sub>	1E-15	1E-15	0	0
H <sub>2</sub> S	0.0000008	0.0000008	0.0000008	0
CO	0.0000005	0.0000005	0.0000005	0

Columns are the same as in Table 1. The initial mixing ratios are abundances at the 1 bar level ( $T=75$  K). The available Gibbs energy from our own code is  $\Phi=0$  J/mol.

\*He was modified from textbook value to ensure mixing ratios summed to 1.

The atmospheric composition of Venus at the surface was taken from the work of Fegley (2014, p 131) and Krasnopolsky and Lefèvre (2013, p 64). The atmospheric composition of Mars at the surface was taken from Lodders and Fegley (1998) but updated with Curiosity rover observations (Mahaffy *et al.*, 2013; Baines *et al.*, 2014). The atmospheric composition of Jupiter at 1 bar was that set forth by Lodders and Fegley (1998) but updated using the compilation of Irwin (2009, pp 100–103). The atmospheric composition of Titan at the surface was taken from the review by Catling (2015). Uranus' atmospheric composition at 1 bar was inferred from the work of Irwin (2009, p 124), Lodders and Fegley (1998), and Catling (2015). Finally, Earth's atmospheric composition was assumed to be that of the US Standard Atmosphere, and the abundance of dissolved ions in average seawater was obtained from the work of Pilson (2012, p 59). Nitrate abundance was obtained from Gruber (2008, p 13).

### 3. Results

Tables 1–7 show equilibrium calculations for the Solar System atmospheres. The format of each table is the same: the first column lists the species present in each body's atmosphere, the second column gives the observed mixing ratios of these species, and the third column is the species abundances at equilibrium, as determined by our Gibbs free energy minimization code. The fourth column is an inde-

pendent validation of our calculations where the equilibrium abundances are determined using the commercial software package Aspen Plus. The equilibrium abundances from our Gibbs energy minimization and from Aspen Plus match very closely in every case. Rows in boldface highlight the species where abundances change during the reaction to equilibrium. Figures 1–7 are the graphical representation of Tables 1–7, respectively. Observed (black bars) and equilibrium (gray bars) abundances of all species for each atmosphere are plotted on a log scale. We only plot the equilibrium abundances from our Gibbs energy minimization calculations and not from Aspen Plus since the differences are barely visible. All equilibrium calculations are performed at observed mean surface temperature and pressure conditions (for terrestrial planets) or at 1 bar and the mean temperature at 1 bar (for giant planets with no surface), unless stated otherwise.

Note that, although the observed abundances in the tables and figures are mixing ratios, the equilibrium abundances do not sum to exactly unity. The equilibrium molar abundances are instead the moles of each species that remain when 1 mol of the observed atmosphere reacts to equilibrium (reaction to equilibrium conserves atoms but does not conserve the number of moles in an atmosphere). We chose not to renormalize the equilibrium abundances to obtain mixing ratios because it was easier to identify which species are involved in reactions from the tables without normalization.

Table 8 shows the available Gibbs energy,  $\Phi$  (defined in Eq. 7) in each planet's atmosphere, and Fig. 8a is a graphical

TABLE 5B. EQUILIBRIUM CALCULATION FOR URANUS' ATMOSPHERE WITH ALL STRATOSPHERIC TRACE SPECIES INCLUDED

<i>Species</i>	<i>Initial mixing ratio</i>	<i>Final abundance (fmincon)</i>	<i>Final abundance (Aspen)</i>	<i>Final – initial abundance (fmincon)</i>
H <sub>2</sub>	<b>0.825</b>	<b>0.82499846</b>	<b>0.8249985</b>	<b>–0.00000154</b>
He*	0.15199857	0.15199857	0.1519986	0
CH <sub>4</sub>	<b>0.023</b>	<b>0.02300054</b>	<b>0.0230005</b>	<b>0.00000054</b>
NH <sub>3</sub>	0.0000001	0.0000001	0.0000001	0
H <sub>2</sub> S	0.0000008	0.0000008	0.0000008	0
CO	<b>0.0000005</b>	<b>1.0905E-19</b>	<b>0</b>	<b>–0.0000005</b>
H <sub>2</sub> O	<b>0.00000006</b>	<b>5.06E-07</b>	<b>0.000000506</b>	<b>0.0000005</b>
C <sub>2</sub> H <sub>6</sub>	<b>0.00000001</b>	<b>3.4293E-19</b>	<b>0</b>	<b>–0.00000001</b>
C <sub>2</sub> H <sub>2</sub>	<b>0.00000001</b>	<b>5.77147E-20</b>	<b>0</b>	<b>–0.00000001</b>

Columns are the same as in Table 1. The calculation is performed at  $P=1$  bar and  $T=75$  K despite the inclusion of stratospheric species to give an upper bound on the free energy at the 1 bar level. The available Gibbs energy from our own code (with all traced species included) is  $\Phi=0.0971$  J/mol.

\*He was modified from textbook value to ensure mixing ratios summed to 1.

TABLE 6. PURELY GAS PHASE EQUILIBRIUM CALCULATION FOR EARTH'S ATMOSPHERE (OCEAN NOT INCLUDED)

<i>Species</i>	<i>Initial mixing ratio*</i>	<i>Final abundance (fmincon)</i>	<i>Final abundance (Aspen)</i>	<i>Final – initial abundance (fmincon)</i>
N <sub>2</sub>	<b>0.773095598</b>	<b>0.773095914</b>	<b>0.7730921</b>	<b>3.16826E-07</b>
O <sub>2</sub>	<b>0.2073826</b>	<b>0.2073791</b>	<b>0.2073829</b>	<b>-3.46776E-06</b>
H <sub>2</sub> O	<b>0.00990082</b>	<b>0.00990473</b>	<b>0.00990473</b>	<b>3.91082E-06</b>
Ar	0.009247366	0.009247366	0.00924737	0
CO <sub>2</sub>	<b>0.000346529</b>	<b>0.000348336</b>	0.000348336	1.8069E-06
Ne	1.79997E-05	1.79997E-05	0.000018	0
He	5.18803E-06	5.18803E-06	0.00000519	-2.5411E-21
CH <sub>4</sub>	<b>1.68314E-06</b>	<b>2.5343E-20</b>	<b>1.13E-48</b>	<b>-1.68314E-06</b>
Kr	1.12869E-06	1.12869E-06	0.00000113	0
H <sub>2</sub>	<b>5.4455E-07</b>	<b>1.0381E-19</b>	<b>4.08E-32</b>	<b>-5.44545E-07</b>
N <sub>2</sub> O	<b>3.16826E-07</b>	<b>3.3401E-19</b>	<b>3.28E-20</b>	<b>-3.16826E-07</b>
CO	<b>1.2376E-07</b>	<b>8.7068E-20</b>	<b>2.18E-32</b>	<b>-1.2376E-07</b>
Xe	8.61371E-08	8.61371E-08	8.61E-08	0
O <sub>3</sub>	<b>4.95041E-08</b>	<b>1.64391E-19</b>	<b>1.97E-30</b>	<b>-4.95041E-08</b>
HCl	9.90082E-10	9.90082E-10	9.9E-10	-6.20385E-25

Columns are the same as in Table 1. The initial mixing ratios are surface abundances ( $T=288.15$  K,  $P=1.013$  bar). The available Gibbs energy for Earth (atmosphere only) from our code is  $\Phi=1.51$  J/mol.

\*Taken US Standard Atmosphere (dry) and added 1% water vapor, then renormalized everything to ensure mixing ratios add to 1.

TABLE 7. MULTIPHASE EQUILIBRIUM CALCULATION FOR EARTH'S ATMOSPHERE-OCEAN SYSTEM ( $T=288.15$  K,  $P=1.013$  BAR)

<i>Species</i>	<i>Initial moles</i>	<i>Final abundance (fmincon)</i>	<i>Final abundance (Aspen)</i>	<i>Final – initial abundance (fmincon)</i>
H <sub>2</sub> O(l)	<b>436.7881549</b>	<b>436.7217842</b>	<b>436.709</b>	<b>-0.066370669</b>
O <sub>2</sub>	<b>0.207382567</b>	<b>0.008094666</b>	<b>1.50756E-05</b>	<b>-0.199287902</b>
N <sub>2</sub>	<b>0.773095598</b>	<b>0.693382141</b>	<b>0.69014709</b>	<b>-0.079713457</b>
<i>NO<sub>3</sub>(-)</i>	<b>0.00023499</b>	<b>0.159662537</b>	<b>0.166132</b>	<b>0.159427547</b>
<i>H(+)</i>	<b>5.10711E-08</b>	<b>0.141936633</b>	<b>0.1484065</b>	<b>0.141936582</b>
H <sub>2</sub> O(g)	<b>0.00990082</b>	<b>0.01229017</b>	<b>0.0119409</b>	<b>0.00238935</b>
Ar	0.009247366	0.009247366	0.009247366	0
CO <sub>2</sub> (g)	<b>0.000346529</b>	<b>0.010835944</b>	<b>0.00943268</b>	<b>0.010489415</b>
Ne	1.79997E-05	1.79997E-05	1.79997E-05	0
He	5.18803E-06	5.18803E-06	5.18803E-06	0
CH <sub>4</sub>	<b>1.68314E-06</b>	<b>2.32128E-13</b>	<b>0</b>	<b>-1.68314E-06</b>
Kr	1.12869E-06	1.12869E-06	1.1287E-06	0
H <sub>2</sub>	<b>5.44545E-07</b>	<b>1.15773E-12</b>	<b>0</b>	<b>-5.44544E-07</b>
N <sub>2</sub> O	<b>3.16826E-07</b>	<b>1.66811E-13</b>	<b>NA</b>	<b>-3.16826E-07</b>
CO	<b>1.2376E-07</b>	<b>1.001E-12</b>	<b>0</b>	<b>-1.23759E-07</b>
Xe	8.61371E-08	8.61371E-08	8.61372E-08	0
O <sub>3</sub>	<b>4.95041E-08</b>	<b>1.43837E-12</b>	<b>0</b>	<b>-4.95027E-08</b>
HCl	<b>9.90082E-10</b>	<b>2.83979E-10</b>	<b>0</b>	<b>-7.06103E-10</b>
<i>Na(+)</i>	<i>3.672916562</i>	<i>3.672916562</i>	<i>3.672917</i>	<i>0</i>
<i>K(+)</i>	<i>0.079974781</i>	<i>0.079974781</i>	<i>0.0799747</i>	<i>0</i>
<i>Mg(2+)</i>	<i>0.413816618</i>	<i>0.413816618</i>	<i>0.4138166</i>	<i>0</i>
<i>Ca(2+)</i>	<i>0.08052309</i>	<i>0.08052309</i>	<i>0.080523</i>	<i>0</i>
<i>Sr(2+)</i>	<i>0.000709668</i>	<i>0.000709668</i>	<i>0.000709669</i>	<i>0</i>
<i>Cl(-)</i>	<b>4.275870063</b>	<b>4.275870063</b>	<b>4.27587</b>	<b>7.061E-10</b>
<i>SO<sub>4</sub>(2-)</i>	<i>0.221125177</i>	<i>0.221125177</i>	<i>0.2211252</i>	<i>0</i>
<i>HCO<sub>3</sub>(-)</i>	<b>0.013911382</b>	<b>9.08865E-08</b>	<b>5.59323E-07</b>	<b>-0.013911291</b>
<i>Br(-)</i>	<i>0.00661104</i>	<i>0.00661104</i>	<i>0.00661104</i>	<i>0</i>
<i>B(OH)<sub>3</sub></i>	<i>0.003258522</i>	<i>0.003258522</i>	<i>NA</i>	<i>0</i>
<i>F(-)</i>	<i>0.000532643</i>	<i>0.000532643</i>	<i>0.000532643</i>	<i>0</i>
<i>CO<sub>2</sub>(aq)</i>	<b>7.598E-05</b>	<b>0.005262085</b>	<b>0.00666488</b>	<b>0.005186105</b>
<i>CO<sub>3</sub>(2-)</i>	<b>0.001762422</b>	<b>7.76602E-14</b>	<b>0</b>	<b>-0.001762422</b>
<i>OH(-)</i>	<b>5.48309E-05</b>	<b>7.33759E-12</b>	<b>4.1902E-12</b>	<b>-5.48309E-05</b>

Columns are the same as in Table 1. The initial mixing ratios are surface abundances. Aqueous species are italicized. The available Gibbs energy for Earth's atmosphere-ocean system from our code is  $\Phi=2326$  J/mol. NA indicates that these species were not included in the Aspen Plus calculation. Note the large changes in nitrate, H(+) ions and oxygen.

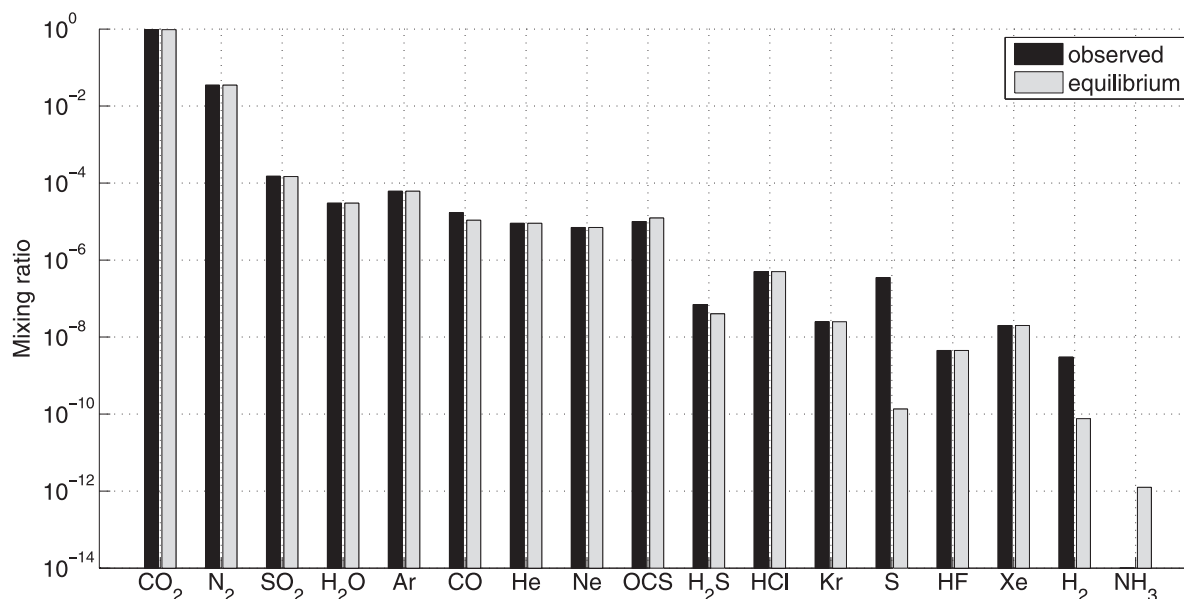


**FIG. 1.** Equilibrium calculation for Venus' atmosphere. The black bars show the observed mixing ratios of all known species in Venus' atmosphere at the surface level ( $T=735.3$  K,  $P=92.1$  bar). The gray bars show the equilibrium abundances of each of these species as determined by our Gibbs free energy minimization code. The black bars are the column 2 abundances in Table 1, and the gray bars are the column 3 abundances in Table 1. Notice the loss of S and reduction of CO and  $H_2S$  at equilibrium.

representation of these results. The second column in Table 8 gives the available Gibbs energy as determined by our own numerical code for Gibbs energy minimization. Column 3 shows the semianalytic approximation of available Gibbs energy that was calculated by choosing key reactions, finding their equilibria independently, and summing the Gibbs energy changes associated with each reaction (see the methods section). Column 4 is the available Gibbs energy in each atmosphere as determined by the commercial software package Aspen Plus. In almost every case, the available Gibbs energies from these three methods are consistent to within a few percent or better. The excellent agreement is encouraging because Aspen Plus uses different thermodynamic databases and models to our Gibbs energy minimization calculations. Column 5 gives the Gibbs free energy of each

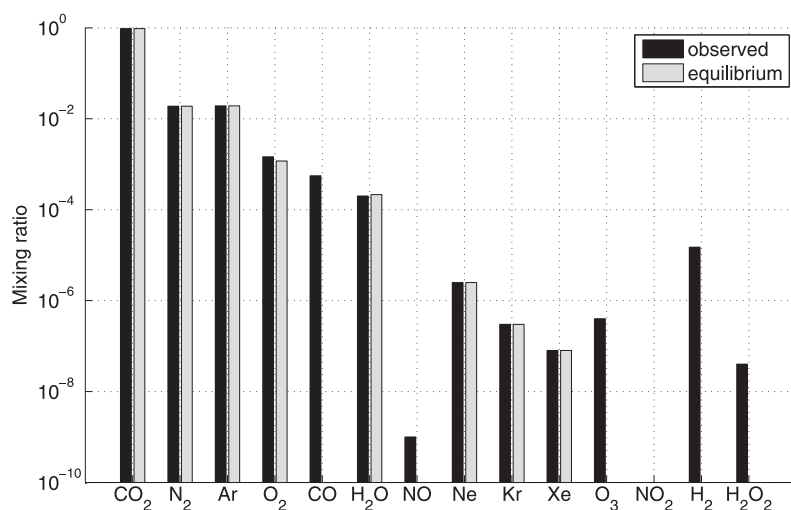
planet as reported by Lovelock (1975). The discrepancies between his results and our results are attributable to much improved knowledge of atmospheric compositions and our more accurate computational techniques (see below).

We now discuss what accounts for the disequilibrium in each atmosphere. We do this by identifying the key gases that are in disequilibrium and describing how the chemical conditions on each body give rise to various disequilibria.

### 3.1. Venus

The disequilibrium in Venus' lower atmosphere is comparatively small, which is expected because the high pressure and temperature favors chemical reactions that push the atmosphere close to equilibrium (Yung and DeMore, 1999, p

**FIG. 2.** Equilibrium calculation for Mars' atmosphere. The black bars show the observed mixing ratios of all known species in Mars' atmosphere at the surface level ( $T=214$  K,  $P=0.006$  bar). The gray bars show the equilibrium abundances of each of these species as determined by our Gibbs free energy minimization code. The black bars are the column 2 abundances in Table 2, and the gray bars are the column 3 abundances in Table 2. Notice the loss of CO and reduction of  $O_2$  at equilibrium. The compensating increase in  $CO_2$  is too small to be visible on this figure.



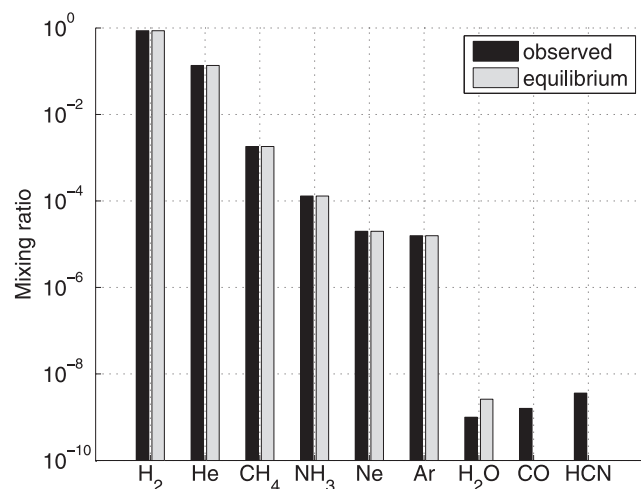


**FIG. 3.** Equilibrium calculation for Jupiter's atmosphere. The black bars show the observed mixing ratios of all known species in Jupiter's atmosphere at the 1 bar level ( $T=165$  K). The gray bars show the equilibrium abundances of each of these species as determined by our Gibbs free energy minimization code. The black bars are the column 2 abundances in Table 3, and the gray bars are the column 3 abundances in Table 3. Notice the loss of CO and HCN at equilibrium.

292). There is little difference between the observed abundances and equilibrium abundances (Fig. 1, Table 1) except for very minor species. Consequently, the available Gibbs energy in Venus' atmosphere is only  $\approx 0.06$  J/mol (Table 8).

The largest contributor to the disequilibrium in Venus' atmosphere (in terms of available energy) is the coexistence of elemental sulfur (S) and carbon dioxide ( $\text{CO}_2$ ). Semianalytic

calculations predict that the following reaction should deplete all the elemental sulfur in Venus' atmosphere:



Gibbs energy minimization calculations confirm that elemental sulfur is absent in equilibrium. The disequilibrium in Venus' atmosphere is maintained by photochemistry; photochemical dissociation of  $\text{SO}_2$  and OCS in the upper atmosphere maintains out-of-equilibrium sulfur chemistry (Yung and DeMore, 1999, p 292).

### 3.2. Mars

The disequilibrium in Mars' atmosphere is large compared to other Solar System atmospheres. The available Gibbs energy in Mars' atmosphere, 136 J/mol, is 1–2 orders of magnitude greater than every other atmosphere we consider except for Earth's atmosphere-ocean system. Figure 2 and Table 2 show several abundant constituents in Mars' atmosphere with observed mixing ratios substantially different from equilibrium abundances.

The largest contributor to disequilibrium in Mars' atmosphere (in terms of available energy) is the coexistence of CO and  $\text{O}_2$ . Both semianalytic and numerical calculations predict that, in equilibrium, all the CO should be oxidized by  $\text{O}_2$  to form  $\text{CO}_2$  by the following reaction:



This is confirmed by the stoichiometry of the change in abundances from the numerical calculation (column 5, Table 2). Reaction to equilibrium decreases the abundance

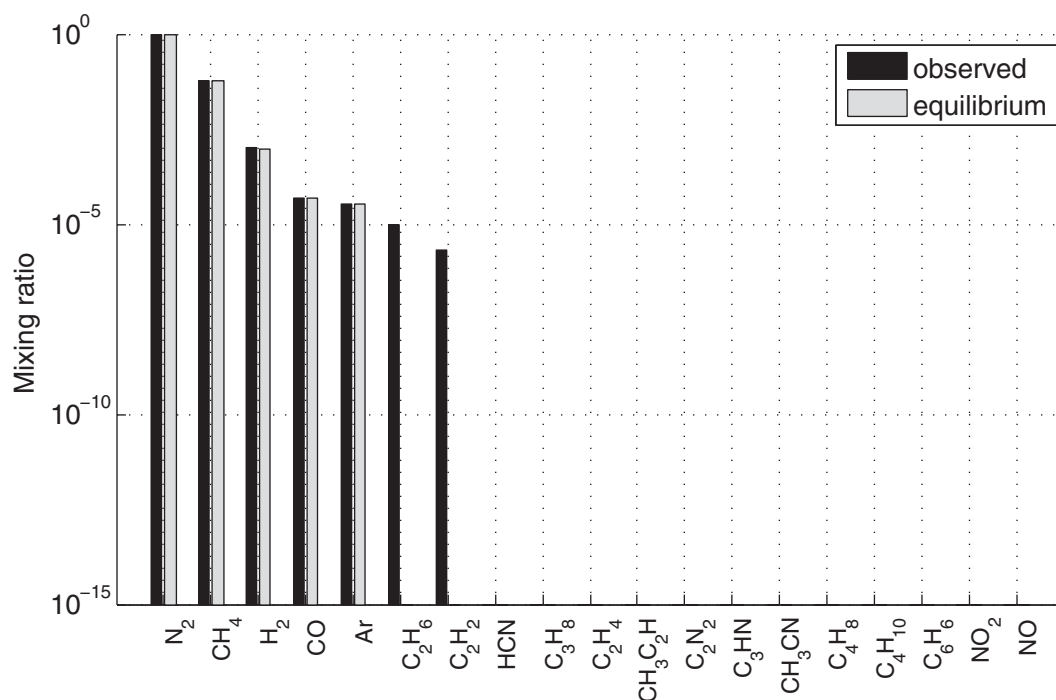


**FIG. 4.** Equilibrium calculation for Titan's atmosphere. The black bars show the observed mixing ratios of all known species in Titan's atmosphere at the surface level ( $T=93.65$  K,  $P=1.46$  bar). The gray bars show the equilibrium abundances of each of these species as determined by our Gibbs free energy minimization code. The black bars are the column 2 abundances in Table 4, and the gray bars are the column 3 abundances in Table 4. Notice the loss of ethane ( $\text{C}_2\text{H}_6$ ) and acetylene ( $\text{C}_2\text{H}_2$ ) at equilibrium.

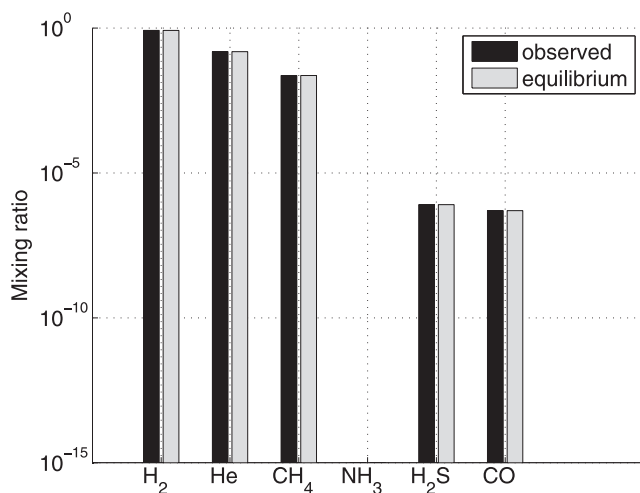


**FIG. 5.** Equilibrium calculation for Uranus' atmosphere. The black bars show the observed mixing ratios of all known species in Uranus' atmosphere at the 1 bar level ( $T=75$  K). The gray bars show the equilibrium abundances of each of these species as determined by our Gibbs free energy minimization code. The black bars are the column 2 abundances in Table 5a, and the gray bars are the column 3 abundances in Table 5a. There is no change in species abundances by reaction to equilibrium.

of O<sub>2</sub> by  $2.8538 \times 10^{-4}$  mol and decreases the abundance of CO by  $5.57 \times 10^{-4}$  mol, that is, almost a 1:2 ratio. The abundance of CO<sub>2</sub> increases by  $5.57 \times 10^{-4}$  mol. The stoichiometry is not exactly the same as Eq. 14 because oxygen is also depleted by reaction with hydrogen gas by the following reaction:

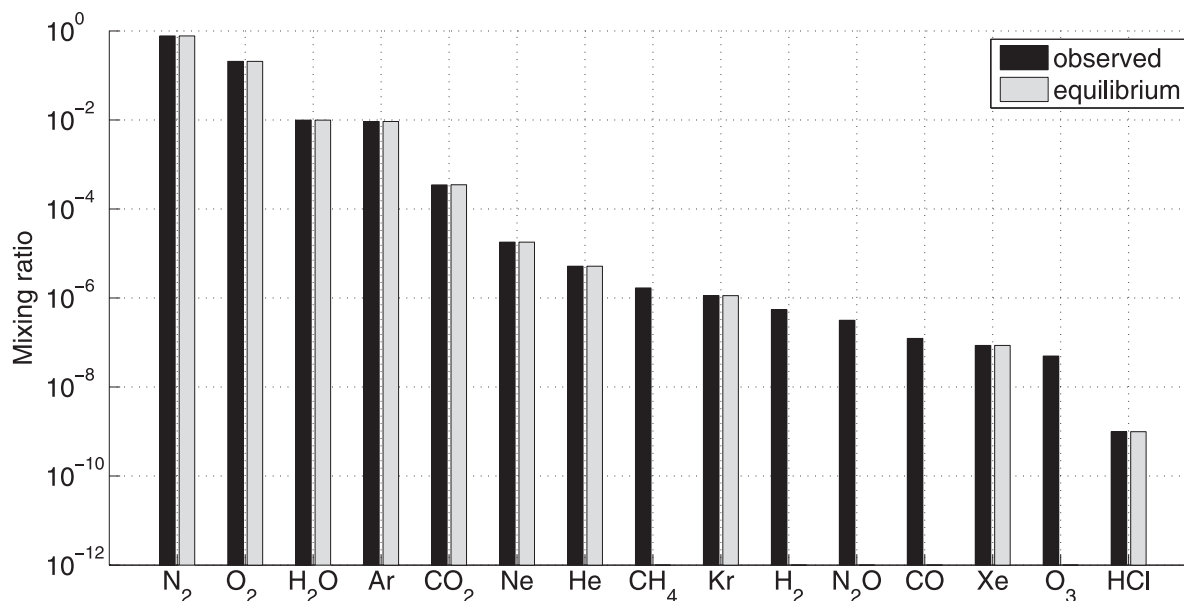


**FIG. 6.** Equilibrium calculation for Earth's atmosphere (not including ocean). The black bars show the observed mixing ratios of all known species in Earth's atmosphere at the surface level ( $T=288.15$  K,  $P=1.013$  bar). The gray bars show the equilibrium abundances of each of these species as determined by our Gibbs free energy minimization code. The black bars are the column 2 abundances in Table 6, and the gray bars are the column 3 abundances in Table 6. Notice the loss of reduced species (CH<sub>4</sub>, H<sub>2</sub>, CO) at equilibrium.

Since numerical calculations indicate that hydrogen decreases by  $0.15 \times 10^{-4}$  mol (column 5, Table 2), this implies molecular oxygen must decrease by  $0.15 \times 10^{-4} / 2 = 0.075 \times 10^{-4}$  mol. Subtracting this decrease from the overall change in oxygen yields  $(2.8538 - 0.075) \times 10^{-4} = 2.7788 \times 10^{-4}$  mol, which is a closer match to the stoichiometry in Eq. 14. The remaining discrepancy is similarly explained by the reaction of ozone to form molecular oxygen:



Disequilibrium in Mars' atmosphere is maintained by photochemistry. The photodissociation of CO<sub>2</sub> continuously replenishes CO in the martian atmosphere (Nair *et al.*, 1994; Zahnle *et al.*, 2008). The martian atmosphere also has an overabundance of H<sub>2</sub> and O<sub>3</sub>, both of which are maintained by photodissociation of water.

The difference between the available Gibbs energy in Mars' atmosphere and the available energy in other photochemically driven atmospheric disequilibria can be partly explained by differences in atmospheric column mass and chemical complexity. Since Mars' atmosphere is more tenuous than other atmospheres, and lacks species (*e.g.*, chlorine-bearing gases) that enable more pathways of catalytic recombination of CO<sub>2</sub>, photochemical reactions have a greater effect on overall composition. In contrast, photochemistry on Venus does not result in large available Gibbs energy per mole of atmosphere because the thick atmosphere along with efficient catalysts buffers its effect on composition. The CO<sub>2</sub> column photodissociation rates on Mars and Venus are comparable,  $2 \times 10^{12}$  molecules/cm<sup>2</sup>/s (Huguenin *et al.*, 1977) and  $7.6 \times 10^{12}$  molecules/cm<sup>2</sup>/s (Bougher *et al.*, 1997, p 448), respectively, whereas the SO<sub>2</sub> column photodissociation rate, or equivalently the H<sub>2</sub>SO<sub>4</sub> production rate, on Venus is  $\sim 5.6 \times 10^{11}$  molecules/cm<sup>2</sup>/s

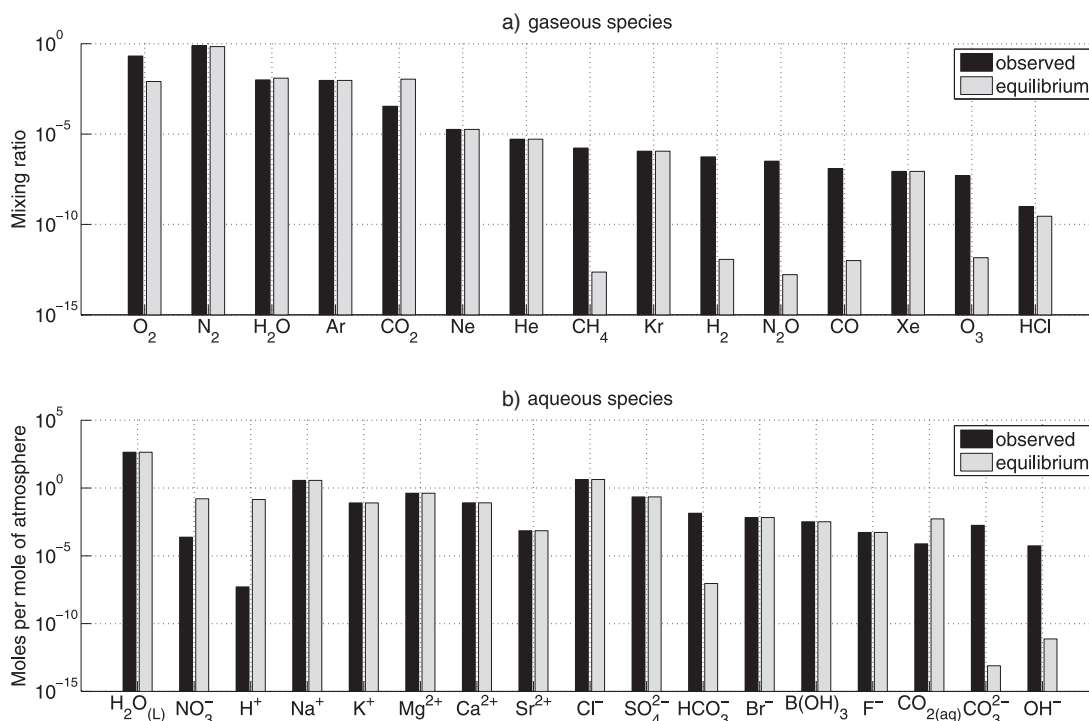


**FIG. 7.** Multiphase equilibrium calculation for Earth's atmosphere-ocean system. The black bars show the observed mixing ratios and abundances of all species in Earth's atmosphere and oceans at the surface level ( $T=288.15$  K,  $P=1.013$  bar). The gray bars show the equilibrium abundances of each of these species as determined by our Gibbs free energy minimization code. The black bars are the column 2 abundances in Table 7, and the gray bars are the column 3 abundances in Table 7. (a) Shows all gas phase species, whereas (b) shows all aqueous species. Notice that in equilibrium there is a large decrease in  $O_2$  since oxygen is converted to nitric acid ( $H^+$  and  $NO_3^-$  increase) by Reaction 21.

(Zhang *et al.*, 2012; Krasnopolsky, 2015). However, the column mass is larger on Venus. The column mass is  $P/g$ , where  $P$  is surface pressure and  $g$  is gravitational acceleration. On Venus, the column mass is  $93.3 \times 10^5$  Pa/ $8.87$  m/s<sup>2</sup> =  $1,051,680$  kg/m<sup>2</sup> (taking the pressure at the mean elevation),

whereas on Mars the column mass is  $600$  Pa/ $3.711$  m/s<sup>2</sup> =  $159.1$  kg/m<sup>2</sup>, so the Venus:Mars ratio is  $1,051,680/159.1 \sim 6,600$ . Whereas Mars has catalytic recombination of  $CO_2$  from only odd hydrogen species, Venus has more efficient catalytic cycles involving Cl, N, and H species for  $CO_2$

**TABLE 8.** COMPARISON OF THE AVAILABLE GIBBS FREE ENERGY,  $\Phi$ , IN SOLAR SYSTEM ATMOSPHERES (DEFINED IN EQUATION 7)

	Available Gibbs energy, $\Phi$ (J/mol of atmosphere) <sup>a</sup>	Validation, $\Phi$ (J/mol of atmosphere)		Lovelock (1975) $\Phi$ (J/mol of atmosphere)
		Semianalytic approximation	Aspen Plus	
Venus	0.059598	0.0565586	0.060099	5
Earth (atm)	1.51348	1.5072	1.52564	Not reported
Earth	2325.76	1723.65 <sup>b</sup>	2348 <sup>c</sup>	55,000
Mars	136.3485	136.8070	136.3506	13
Jupiter	0.001032077	0.00103205	0.0010228	<1
Titan	1.2126495	1.212617	1.208787	Not reported
Uranus <sup>d</sup>	0.0971394	0.0983	0.09713801	Not reported

The second column gives  $\Phi$  for each atmosphere as determined by our Gibbs energy minimization calculations. The third column is our semianalytic approximation of the available Gibbs energy calculated from summing the Gibbs energy changes associated with key reactions (see main text and Appendix D). The fourth column is an independent verification of  $\Phi$  using the commercial software package Aspen Plus. The fifth report compares our values to those of Lovelock (1975).

<sup>a</sup>Calculated at surface pressure and temperature for Venus, Earth, Mars and Titan. Calculated at 1 bar and  $T=165$  K and  $T=75$  K for Jupiter and Uranus, respectively.

<sup>b</sup>The discrepancy between the numerical and semianalytic results for Earth is expected because the semianalytic approximation does not take into account changing water activity. See the main text and Table 9 for a more detailed explanation.

<sup>c</sup>Note that different electrolyte models in Aspen Plus produce slightly different Gibbs energy changes. The available Gibbs energy using the Electrolyte Non-Random Two Liquid (ELECRTL) model is  $2348$  J/mol, whereas the Pitzer electrolyte returns a Gibbs energy change of  $2205$  J/mol (see Appendix E for a full description of multiphase Aspen Plus calculations).

<sup>d</sup>Unrealistically includes stratospheric species and gaseous water vapor, so this is an upper bound on free energy.

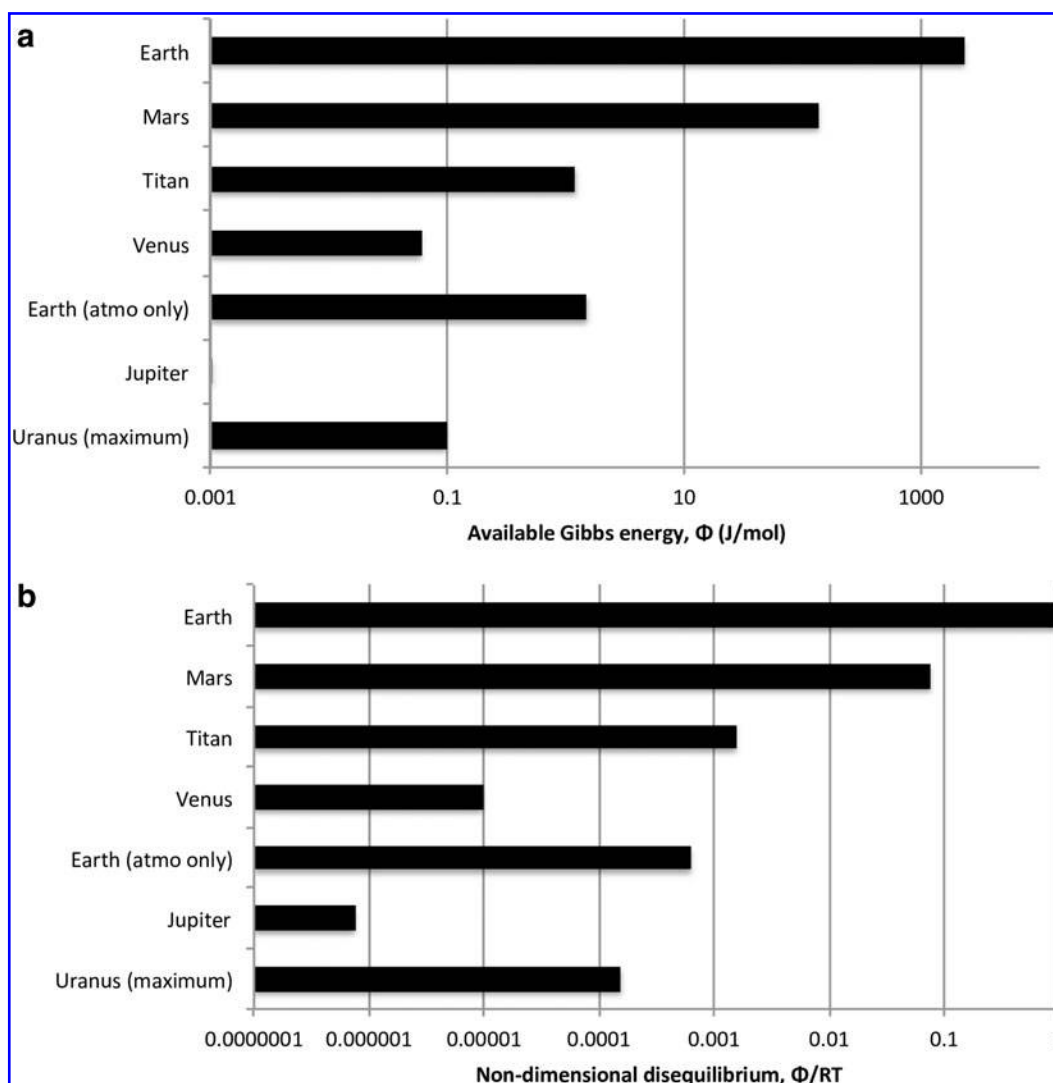


**FIG. 8.** Comparison of the available Gibbs free energy,  $\Phi$ , in Solar System atmospheres as determined by our Gibbs free energy minimization calculations. The available Gibbs free energies in (a) correspond to the second column in Table 8. The free energy in the Earth atmosphere-ocean system is more than an order of magnitude greater than any other planetary atmosphere in the Solar System. (b) gives the dimensionless free energy for each planet's atmosphere (available Gibbs energy  $\Phi$  divided by  $RT$ ). This roughly corrects for the fact that the inner planets receive more free energy from the Sun that is available to drive chemical disequilibrium. Equilibria are calculated at surface pressure and temperature for Venus, Earth, Mars, and Titan, and at 1 bar and  $T=165$  K and  $T=75$  K for Jupiter and Uranus, respectively.

recombination (Yung and DeMore, 1999, pp 249, 288), such that  $O_2$  on Venus has an upper limit concentration  $<0.3$  ppmv. Consequently, the products of  $CO_2$  dissociation do not significantly influence the disequilibrium on Venus; instead, sulfur chemistry makes the dominant contribution, as discussed earlier. The net result is that the available free energy in Venus' atmosphere is  $\sim 2000$  times smaller than that of Mars (Table 8).

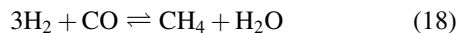
Note that Mars' atmospheric composition varies seasonally via  $CO_2$  exchange with polar caps, and on longer timescales obliquity cycles will modulate atmospheric  $CO_2$  due to regolith adsorption. However, these changes in atmospheric composition are unlikely to have a large effect on the available energy in Mars' atmosphere. The total  $CO_2$  reservoir in the regolith and the polar ice is equivalent to 5–30 mbar  $CO_2$  (Covey *et al.*, 2013, p 171). Zahnle *et al.* (2008) used a 1-D photochemical model to compute self-

consistent martian atmospheres with  $pCO_2$  varying from 1 to 100 mbar, thereby encompassing the range of atmospheric variability from seasonal and obliquity variations. We computed the available energy for this range of photochemical outputs and found that it was less than 200 J/mol regardless of  $pCO_2$ . Although the photochemical model calculates the water volume mixing ratio from a specified relative humidity,  $H_2O$  is redox neutral, so changing its abundance will not have a large effect on available energy.

### 3.3. Jupiter

The disequilibrium in Jupiter's atmosphere at the 1 bar level is very small compared to other atmospheres in the Solar System ( $\approx 0.001$  J/mol). The observed mixing ratios and equilibrium abundances (Table 3, Fig. 3) are virtually identical; the largest changes are at the parts per billion

level. The small disequilibrium in Jupiter's atmosphere is attributable to the coexistence of HCN with  $H_2$  and the coexistence of CO with  $H_2$ . Both numerical and semi-analytic calculations predict that HCN and CO should be completely depleted in equilibrium by the following reactions



This is confirmed by the stoichiometry of the change in abundances from the numerical calculation (column 5, Table 3): HCN and CO abundances decrease by  $3.6 \times 10^{-9}$  and  $1.6 \times 10^{-9}$  mol, respectively, whereas  $NH_3$  and  $H_2O$  abundances increase by  $3.6 \times 10^{-9}$  and  $1.6 \times 10^{-9}$  mol, respectively. Based on these numbers and Eqs. 17 and 18, we would predict that  $CH_4$  abundance should increase by  $(3.6 + 1.6) \times 10^{-9} = 5.2 \times 10^{-9}$  mol, and that  $H_2$  abundance should decrease by  $3 \times (3.6 \times 10^{-9} + 1.6 \times 10^{-9}) = 1.56 \times 10^{-8}$  mol. These predictions exactly match the observed changes in these species in Table 3.

It is not surprising that Jupiter's atmosphere is very close to equilibrium. Photochemically produced disequilibrium species are vigorously mixed into the high-temperature interior (1000 K), where they are hydrogenated to reform equilibrium species (Lewis, 2012, pp 209–212). The small disequilibrium that remains is attributable to a combination of deeper vertical mixing, material delivery, and photochemistry. CO is thermodynamically favored in the very high-temperature interior, and deep vertical mixing delivers it to the upper atmosphere (Prinn and Barshay, 1977), although some infall of material from space is required to explain observed CO abundances (Bézard *et al.*, 2002). HCN is also thermodynamically favored in the interior, but observed abundances are best explained by photochemical sources (Kaye and Strobel, 1983).

We repeated the equilibrium calculation for Jupiter at the 1 mbar level. This is of interest for exoplanet characterization since infrared spectroscopy may be limited to probing the millibar level of jovian-like atmospheres due to thick clouds or hazes. The mean temperature at 1 mbar is approximately equal to the temperature at 1 bar due to the temperature inversion in Jupiter's stratosphere; consequently any difference in available Gibbs energy can be ascribed to changing mixing ratios. Using stratospheric species abundances of Irwin (2009, p 101), we found the available Gibbs energy in Jupiter's atmosphere at 1 mbar to be 0.35 J/mol. This disequilibrium can be ascribed to photochemically replenished organics such as  $C_2H_6$  and to a lesser extent  $C_2H_2$  and  $C_2H_4$ .

### 3.4. Titan

The moderate disequilibrium in Titan's atmosphere ( $\approx 1.2$  J/mol) is also driven by photochemistry. Both ethane ( $C_2H_6$ ) and acetylene ( $C_2H_2$ ) exist in Titan's atmosphere, whereas semianalytic and numerical calculations predict that these species should be depleted in equilibrium by reactions with  $H_2$  to form  $CH_4$ :

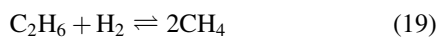


Table 4 confirms this stoichiometrically: ethane and acetylene abundances decrease by  $1 \times 10^{-5}$  and  $2 \times 10^{-6}$ , respectively, by reaction to equilibrium (Table 4). From the equations above, this would imply that  $CH_4$  abundance should increase by  $2 \times (1 \times 10^{-5} + 2 \times 10^{-6}) = 2.4 \times 10^{-5}$ , whereas hydrogen abundance should decrease by  $3 \times 2 \times 10^{-6} + 1 \times 10^{-5} = 1.6 \times 10^{-5}$ . These predictions exactly match the observed changes in these species in Table 4.

We have not included Titan's hydrocarbon lakes in this calculation for several reasons. First, the thermodynamics of cold hydrocarbon solutions is beyond the scope of this study and poorly known. Second, the composition of lakes on Titan and the degree to which they are variable are unknown. Third, current hypothetical estimates of lake composition (Cordier *et al.*, 2009; Glein and Shock, 2013) are based on purely thermodynamic equilibrium models and so are inappropriate for revealing disequilibrium. The total volume of Titan's lakes is estimated to be  $32,000 \text{ km}^3$  (Lorenz *et al.*, 2014). If we assume the lake density is  $654 \text{ kg/m}^3$ , which is the density of liquid ethane at 92.5 K (Younglove and Ely, 1987), then the total mass of the lakes is  $2.1 \times 10^{16} \text{ kg}$ . The surface pressure on Titan is 1.5 bar, the surface area is  $8.3 \times 10^7 \text{ km}^2$ , and the surface gravity is  $1.35 \text{ ms}^{-2}$ . This implies the mass of the atmosphere is  $(8.3 \times 10^7 \times 1000^2 \text{ m}^2) \times (10^5 \times 1.5 \text{ Pa}) / (1.35 \text{ ms}^{-2}) = 9.2 \times 10^{18} \text{ kg}$ . Thus, the mass of the lakes is 0.2% the mass of Titan's atmosphere. Disequilibrium species at the parts-per-thousand level can impact the available energy, as evidenced by the CO- $O_2$  pairing in Mars' atmosphere. Consequently, if Titan's lakes are in chemical disequilibrium with the atmosphere, then the available Gibbs energy of the total fluid reservoir may be larger than the atmosphere-only result we report here.

### 3.5. Uranus

Observational knowledge of Uranus' atmosphere is limited, so it is difficult to calculate disequilibrium at the 1 bar level. Table 5a shows the observed abundances at 1 bar; there is insufficient diversity of molecular species for any reactions to occur. The observed composition is the same as the equilibrium composition, and the available Gibbs energy in Uranus' troposphere is nominally 0 J/mol. In reality, there are probably trace species at 1 bar that contribute to a small disequilibrium. To place an upper bound on the disequilibrium in Uranus' atmosphere, we included trace species from the stratosphere in our calculations (Table 5b). Of course, the stratosphere for most planets with thick atmospheres and shortwave stratospheric absorbers is located vertically above the  $\sim 0.1$  bar level (Robinson and Catling, 2014) and so is not at the 1 bar level that we use for Gibbs energy calculations. Even so, when semianalytic and numerical calculations are repeated for this case, we find the maximum disequilibrium in Uranus' atmosphere is still comparatively small, 0.097 J/mol.

### 3.6. Saturn and Neptune

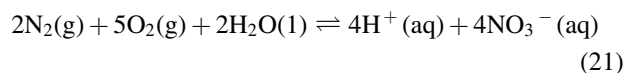
Saturn and Neptune were excluded from our analysis because of their close similarity to Jupiter and Uranus, respectively. Essentially, in Jupiter and Uranus, we chose a representative of the gas and ice giants, respectively.

### 3.7. Earth

We calculated the disequilibrium in Earth's atmosphere for two different cases. Firstly, we considered only Earth's atmosphere (Fig. 6, Table 6). There are minor differences between the observed atmospheric composition and the equilibrium composition. The largest contributor to gas phase disequilibrium in Earth's atmosphere is the coexistence of  $O_2$  and  $CH_4$ , and the available Gibbs energy in the atmosphere is only 1.5 J/mol, which is not unusual compared to other Solar System atmospheres. The  $O_2$  and  $CH_4$  couple contributes  $\sim 90\%$  of this gas phase disequilibrium (1.3 J/mol).

Next, we consider the multiphase equilibrium calculation that includes Earth's atmosphere and oceans with dissolved ion species (Fig. 7, Table 7). In this case, the disequilibrium in Earth's atmosphere-ocean system is very large; the available Gibbs energy is 2326 J/mol of atmosphere.

The large disequilibrium is attributable to the coexistence of  $N_2$ ,  $O_2$ , and liquid water. Both numerical and semi-analytic calculations predict that these three species should react to form nitrate and hydrogen ions according to the following reaction:



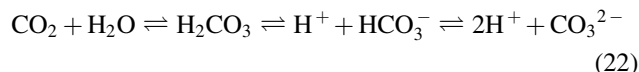
In equilibrium, most of the oxygen in Earth's atmosphere reacts to form hydrogen ions and nitrate (Table 7). It has been known for many decades that the coexistence of  $N_2$ ,  $O_2$ , and  $H_2O$  is the largest contributor to disequilibrium in Earth's atmosphere-ocean system (Lewis and Randall, 1923; Hutchinson, 1954, p 399; Sillén, 1966; Lovelock, 1975). However, this is the first time the free energy associated with that disequilibrium has been accurately calculated. Lovelock (1975) reported that the free energy in Earth's atmosphere-ocean system was  $5.5 \times 10^4$  J/mol (Table 8), which is over an order of magnitude larger than our result. He did not describe his methodology, but we suspect that he assumed the Gibbs energy of the  $N_2$ - $O_2$ - $H_2O$  reaction does not change as the reaction proceeds, and simply multiplied the Gibbs energy of the reaction (at observed abundances) by the number of moles of oxygen in Earth's atmosphere. This approach also assumes the reaction goes to completion with total  $O_2$  removal rather than equilibrium. Preliminary analyses by the authors of this study (Catling and Bergsman, 2009, 2010) reached a similar result using this methodology. Both the semianalytic and numerical calculations in this study account for the fact that the Gibbs energy of the reaction diminishes rapidly as oxygen in the atmosphere is depleted, so the available Gibbs energy in Earth's atmosphere-ocean system, 2326 J/mol, is smaller than previously reported.

Of course, the equilibrium metric is only a hypothetical way of assessing untapped free energy. In reality,  $O_2$  also reacts with surface minerals (oxidative weathering) and would be even more depleted with additional free energy if solids were included in the equilibrium model. But we restrict ourselves to gas and gas-liquid equilibrium because those are tractable ways of comparing planets that are tied to quantities that can be observed remotely (see more in the discussion section).

We confirmed that the available Gibbs energy in Earth's atmosphere-ocean system is attributable to Reaction 21 by repeating the multiphase calculation but excluding  $H^+$  and

$NO_3^-$ . In this case the available Gibbs energy is only 6 J/mol. If we only include the five most important species ( $N_2$ ,  $O_2$ ,  $H_2O$ ,  $H^+$ , and  $NO_3^-$ ) in multiphase equilibrium calculations, then the available Gibbs energy change is 1812 J/mol (note this includes the effects of changing water activity—see below for details). The difference between this and the total available energy for the Earth system is attributable to carbon-bearing species.

The dissolution of hydrogen ions and nitrate in the ocean by Eq. 21 acidifies the ocean, which affects the carbonate- $CO_2$  system. By Le Châtelier's principle, as the ocean is acidified, carbon in the form of carbonate and bicarbonate ions converts to atmospheric  $CO_2$  and dissolved  $CO_2$ :



This reaction shifts to the left as the concentration of hydrogen ions is increased. The Gibbs energy change associated with this shift adds to the overall Gibbs energy change in Earth's atmosphere-ocean system. Additionally, the dissolution of nitrate and hydrogen ions in water decreases the water activity, which further contributes to the overall Gibbs energy change. If water activity is held fixed, then the available Gibbs energy for Earth is around 600 J/mol less than if water activity is included.

Validating our results for the Earth atmosphere-ocean system is more complex than for gas phase systems. This is because the semianalytic method we have adopted does not account for the decrease in water activity due to increased nitrate and hydrogen ion abundances. Rather than attempt to compute water activities analytically, we calculated the Gibbs energy change associated with Eq. 21 in isolation and compared this to the numerical Gibbs energy minimization calculation using only the five species in this reaction and with water activity fixed to equal 1. The available Gibbs energies for these two cases are shown in Table 9; the two values agree to within 1%. Next, we computed the available energy semianalytically using both Reaction 21 and two key reactions that involve carbon-bearing species (see Appendix D). This was compared to the numerical Gibbs energy minimization calculation for the same set of species with the

TABLE 9. SEMIANALYTIC VALIDATION OF THE NUMERICAL CALCULATION OF THE AVAILABLE GIBBS FREE ENERGY,  $\Phi$ , IN THE EARTH ATMOSPHERE-OCEAN SYSTEM

Species included in calculation	Available energy, $\Phi$ (J/mol)	
	Semianalytic approximation	Numerical calculation (fmincon)
$N_2$ , $O_2$ , $H_2O$ , $H^+$ , and $NO_3^-$ only. Water activity = 1.	1051	1059
Five species above plus carbon-bearing species. Water activity = 1.	1723	1716
All species and water activity included.	NA	2326

water activity set equal to 1. In this case, the available Gibbs energy values also agreed to within 1% (Table 9). The difference between this result and the complete numerical calculation can be explained by the effect of water activity. In the numerical calculations, the water activity decreases from 0.981877 to 0.981284 from observed to equilibrium state. Following Eq. 9, this corresponds to a change in Gibbs free energy of

$$\begin{aligned} \Delta G &\approx n_w RT (\ln \gamma_1 - \ln \gamma_2) \\ &= 436 \times 8.314 \times 288.15 (-0.01828897 + 0.01889366) \\ &= 631 \text{ J/mol} \end{aligned} \quad (23)$$

Here,  $n_w = 436$  mol of  $\text{H}_2\text{O}(\text{l})$  per mole of atmosphere, which is derived from the moles of  $\text{H}_2\text{O}$  in the ocean [ $7.67 \times 10^{22} = 1.38 \times 10^{21}$  kg/(0.018 mol  $\text{H}_2\text{O}/\text{kg}$ )] and moles of air ( $1.76 \times 10^{20}$ ) as their ratio,  $436 = 7.67 \times 10^{22}/1.76 \times 10^{20}$ . The value of 631 J/mol is approximately equal to the difference between the numerical calculation including carbon species (water activity = 1) and the full numerical calculation (2326 – 1716 = 610 J/mol).

We conclude that the total available Gibbs energy of the Earth atmosphere-ocean, 2326 J/mol, can be explained almost completely by the nitrate reaction (1059 J/mol), the change in carbon-bearing species due to ocean acidification (657 J/mol), and the associated change in water activity (610 J/mol). This conclusion is supported by both numerical and semianalytic calculations. We do not account for the pressure decrease in our Gibbs energy calculations from depleting the atmosphere of oxygen given that Gibbs energy is defined for a system at constant pressure and temperature. Our multiphase calculations for Earth should be treated as a constant-pressure approximation.

Although the coexistence of  $\text{O}_2$  and  $\text{CH}_4$  is the largest contributor to disequilibrium for a calculation of Earth's atmosphere excluding the oceans, this pair provides a small contribution to the disequilibrium in the total atmosphere-ocean system. If methane is excluded from the Earth atmosphere-ocean equilibrium calculation, then the available Gibbs energy changes from 2325.76 J/mol to 2324.46 J/mol. Similarly, semianalytic calculations for the reaction  $2\text{O}_2 + \text{CH}_4 \rightleftharpoons \text{CO}_2 + 2\text{H}_2\text{O}$  yield a Gibbs energy change of only 1.3 J/mol. Methane does not contribute much to thermodynamic disequilibrium because of its low abundance of 1.7 ppmv (in the US Standard Atmosphere, noting that anthropogenic emissions mean that the current mean global abundance is slightly higher at  $\sim 1.8$  ppmv). This does not imply that the  $\text{O}_2$ - $\text{CH}_4$  disequilibrium is unimportant for life-detection purposes. A compelling argument for biogenic fluxes can be made from the coexistence of  $\text{O}_2$  and  $\text{CH}_4$  in Earth's atmosphere based on kinetic lifetimes. However, the  $\text{O}_2$ - $\text{CH}_4$  pairing is not an important contributor to the available Gibbs energy of thermodynamic disequilibrium in Earth's atmosphere-ocean system.

To express available Gibbs energy as a dimensionless metric, Fig. 8b plots the available Gibbs free energy in each planet's atmosphere normalized by  $RT$ , where  $T$  is the mean temperature for each planet. The value  $RT$  is the molar thermal energy and depends on solar flux along with Bond albedo and greenhouse effect. Thus, the normalization is a first-order and rough correction for the fact that the inner

planets receive more free energy input from the Sun that can drive disequilibrium. Figure 8b is similar to Fig. 8a because surface or 1 bar temperatures vary by an order of magnitude at most, whereas the available Gibbs energies vary by many orders of magnitude. In Fig. 8b, Earth stands out as the only planet in the Solar System with chemical disequilibrium comparable in magnitude to thermal energy.

## 4. Discussion

### 4.1. Interpretation of thermodynamic disequilibrium

Earth is unique in the Solar System as the only planet with both a large disequilibrium in its atmosphere-ocean system and a productive surface biosphere (with the caveat that we have not included Titan's lakes in our calculations). This disequilibrium is maintained by life. Atmospheric  $\text{O}_2$  is produced almost exclusively by oxygenic photosynthesis, and atmospheric  $\text{N}_2$  is regulated by bacterial nitrification and denitrification. Were denitrification to shut off and biological N fixation left to operate, the  $\text{N}_2$  lifetime would be  $\sim 10$  million years (Jacob, 1999, Chapter 6).

In the absence of any biogenic fluxes or geological oxygen sinks such as oxidative weathering, Reaction 21 would proceed slowly due to lightning, eventually depleting the atmosphere of oxygen [there is some abiotic denitrification, but the flux is very small compared to biological denitrification (Devol, 2008)]. The modern rate of production of nitrogen oxide radicals  $\text{NO}_x$  ( $= \text{NO} + \text{NO}_2$ ) from lightning is 2–20 Tg(N)/year (Rakov and Uman, 2007). OH radicals or ozone further oxidize  $\text{NO}_x$  species into nitrate that ends up on Earth's surface. Given that the mixing ratio of  $\text{N}_2$  decreases by approximately 0.08 in our equilibrium calculations, and that the total number of moles of air in the atmosphere is  $1.76 \times 10^{20}$ , this implies that  $1.408 \times 10^{19}$  mol of  $\text{N}_2$  ( $2.816 \times 10^{19}$  mol of N) are converted to nitrate by reaction to equilibrium. Therefore, it would take approximately  $2.816 \times 10^{19}/(2-20 \times 10^{20}/14) = 20-200$  million years for atmospheric oxygen to be depleted by lightning and converted to nitrate. The coexistence of oxygen, nitrogen, and liquid water in Earth's atmosphere-ocean system is thus evidence a biosphere acting over geological timescales. Capone *et al.* (2006) also noted that denitrification sustains atmospheric nitrogen on Earth and that, although there are abiotic pathways that deplete  $\text{N}_2$  (namely, lightning), nitrates are not easily converted back to  $\text{N}_2$  abiotically. In contrast, Kasting *et al.* (1993) argued that on prebiotic Earth most of Earth's nitrogen would have resided in the atmosphere in steady state. This is because nitrate is reduced to ammonia in mid-ocean-ridge hydrothermal systems, which may then return to the atmosphere and be photochemically converted back to  $\text{N}_2$ . In practice, however, the reduction of nitrate will also yield ammonium (Bada and Miller, 1968; Smirnov *et al.*, 2008), which will be subsequently sequestered into clay minerals and thereby removed from the atmosphere-ocean reservoir (Summers *et al.*, 2012).

It is worth considering why this large disequilibrium exists in Earth's atmosphere-ocean system and whether we would expect other biospheres to generate large disequilibria. In some respects, Earth's large disequilibrium is surprising since life typically exploits environmental free energy gradients rather than generate them. In fact, the  $\text{O}_2$ - $\text{N}_2$ -water disequilibrium is an incidental by-product of

oxygenic photosynthesis. In addition to producing molecular oxygen, oxygenic photosynthesis also produces large quantities of organic carbon that are buried in sediments. Despite ongoing nitrification and the thermodynamic favorability of Reaction 21, nitrate does not accumulate and deplete the atmosphere of oxygen. This is because denitrifying microbes in anoxic sediments exploit the redox gradient that exists between reduced organic carbon and nitrate (Devol, 2008). Without oxygenic photosynthesis producing both O<sub>2</sub> and reduced carbon, Earth's atmosphere-ocean disequilibrium would not persist.

In our calculated equilibrium for the Earth atmosphere-ocean system, the molar abundance of H<sup>+</sup> ions is 0.14 mol per mole of atmosphere, which corresponds to an ocean pH of 1.7. Lewis and Randall (1923, pp 567–568) recognized that the equilibrium state of Earth's atmosphere-ocean system would be acidic:

Even starting with water and air, we see ... that nitric acid should form ... until it reaches a concentration ... where the calculated equilibrium exists. It is to be hoped that nature will not discover a catalyst for this reaction, which would permit all of the oxygen and part of the nitrogen of the air to turn the oceans into dilute nitric acid.

However, the low pH equilibrium state that we obtain is unlikely to be the state actually realized if life disappeared from Earth, volcanic fluxes ceased, and the system relaxed to equilibrium. In practice, acidic ocean pH from nitrate dissolution would be buffered by reaction with the crust, for instance by delivery of cations from continental weathering or weathering of seafloor basalt. Nevertheless, we have done calculations where the ocean pH is buffered to pH 8.2, and the Gibbs free energy from reaction to equilibrium is several times larger than our original result.

This discussion highlights the point that we have not included any interactions with solid states of matter in our equilibrium calculations. If Earth's atmosphere-ocean system were allowed to relax to equilibrium, then almost all the atmospheric O<sub>2</sub> would react with the crust via oxidative weathering. There would be a large Gibbs energy change associated with this crustal oxidation. Additionally, there is a large disequilibrium between organic carbon and ferric iron in the crust, both of which have accumulated over time because of photosynthesis and the escape of hydrogen to space (Catling *et al.*, 2001). Although there are  $3.7 \times 10^{19}$  mol of O<sub>2</sub> in the atmosphere and oceans, there are  $5.1 \times 10^{20}$  mol O<sub>2</sub> equivalent Fe<sup>3+</sup> and sulfate in sedimentary rocks, and  $1.6\text{--}2.5 \times 10^{21}$  mol O<sub>2</sub> equivalent excess Fe<sup>3+</sup> in igneous and high-grade metamorphic rocks (Catling *et al.*, 2001; Sleep, 2005; Hayes and Waldbauer, 2006). These crustal oxidants are in disequilibrium with the  $\leq 1.3 \times 10^{21}$  mol O<sub>2</sub> equivalent reduced organic carbon in the crust (Wedepohl, 1995; Catling *et al.*, 2001). Thus, we expect the disequilibrium in Earth's entire crustal reservoir to be several orders of magnitude greater than the disequilibrium in the atmosphere-ocean system in isolation.

However, we chose to exclude interactions with solid phases since we are interested in disequilibrium as a biosignature for exoplanets; the composition of exoplanet crustal material will not be accessible to remote sensing. Instead, our available Gibbs energy metric captures disequilibrium in the gaseous and aqueous phases. In principle,

atmospheric composition and the presence of an ocean can be inferred from future telescope observations.

The thermodynamic biosignature metric described in this paper is complementary to kinetic biosignature metrics concerning the fluxes and timescales of gases that should quickly react, such as coexisting oxygen and methane. For example, if the atmospheric abundances of oxygen and methane can be observed, and the abiotic sinks for oxygen and methane can be estimated, then the magnitude of source fluxes required to maintain steady state can be estimated. Biogenic processes may be invoked if these source fluxes are implausibly large compared to all known abiotic sources of oxygen and methane. We calculate that in thermodynamic chemical equilibrium, all CH<sub>4</sub> would be absent from Earth's atmosphere (see results). The average lifetime of a CH<sub>4</sub> molecule from photochemical models is  $\sim 10$  years, so we can deduce an estimate of the required CH<sub>4</sub> flux. For consumption of 1.7 ppmv CH<sub>4</sub> in 10 years:  $(1.7 \times 10^{-6}) \times (1.8 \times 10^{20} \text{ mol air}) / (10 \text{ years}) = 3.1 \times 10^{13}$  mol CH<sub>4</sub>/year flux. The magnitude of this flux is large and on Earth dominantly ( $\sim 90\%$ ) biogenic (Kirschke *et al.*, 2013).

These flux arguments can be extended to estimate the surface biomass (Seager *et al.*, 2013) or the minimal driving power (Simoncini *et al.*, 2013) required to maintain steady-state atmospheric abundances. These estimates could provide additional insight into whether the observed disequilibrium is plausibly biogenic in origin; for instance, if the biomass estimate is unreasonably large, or if the driving power is comparable to abiotic processes, the inference to biology is weakened.

It should be noted that our gas phase calculations for Earth are entirely consistent with the minimal driving power calculations of Simoncini *et al.* (2013). We determined that the available energy from the CH<sub>4</sub> and O<sub>2</sub> reaction in Earth's atmosphere is 1.3 J/mol of atmosphere (see the results section). Because there are  $1.8 \times 10^{20}$  mol in Earth's atmosphere, this implies the total available energy in Earth's atmosphere due to this pairing is  $1.3 \times 1.8 \times 10^{20} = 2.34 \times 10^{20}$  J. The turnover lifetime of CH<sub>4</sub> in Earth's atmosphere is approximately 10 years (Dlugokencky *et al.*, 1998; Prinn *et al.*, 2001). If we assume that all the CH<sub>4</sub> in Earth's atmosphere is oxidized in 10 years ( $3.15 \times 10^8$  s) on average, then the "power" from the CH<sub>4</sub>-O<sub>2</sub> reaction according to our calculations will be the free energy release spread over this time:  $\text{Power} = (2.34 \times 10^{20}) / (3.15 \times 10^8) = 0.7 \text{ TW}$ . Simoncini *et al.* (2013) also found the power required to maintain the O<sub>2</sub>-CH<sub>4</sub> disequilibrium to be 0.7 TW.

We have shown that large thermodynamic disequilibria coincide with surface biology in the Solar System, but whether chemical disequilibrium would be a useful metric for identifying exoplanet biospheres remains an open question. In principle, low-flux abiotic processes with slow kinetics might maintain a large atmospheric chemical disequilibrium. For example, we might imagine H<sub>2</sub> and N<sub>2</sub> to coexist in thermodynamic disequilibrium for long timescales with very small replenishing fluxes (assuming a super Earth with sufficient gravity to retain hydrogen). In practice, however, there are few kinetic barriers to gas phase reactions at Earth-like temperatures and pressures, so sizeable disequilibria from abiotic processes may be rare. In future work, it would be helpful to apply this metric to model

exoplanet atmospheres to determine whether there are any plausible false-positive scenarios, that is, dead worlds with large available Gibbs energy. For example, a Mars-like atmosphere with different CO, O<sub>2</sub>, and H<sub>2</sub> abundances—perhaps due to elevated UV irradiation or different outgassed species—could perhaps have a large thermodynamic disequilibrium in the absence of life. Future work should also investigate how abiotic disequilibrium in Solar System atmospheres may have varied since 4.56 Ga.

#### 4.2. Practicality of thermodynamic disequilibrium as exoplanet biosignature

The main advantage of using thermodynamic disequilibrium for biosphere detection over kinetic metrics is that it requires minimal auxiliary assumptions. Whereas kinetic arguments require abiotic surface sinks to be estimated, the calculation of gas phase chemical equilibrium in a planet's atmosphere requires only bulk atmosphere abundances, surface temperature, and pressure; future observations could be used to infer all three of these (Des Marais *et al.*, 2002; Misra *et al.*, 2014). Schwieterman *et al.* (2015) recently demonstrated that it is possible to constrain the abundance of molecular nitrogen due to its tendency to form N<sub>2</sub>-N<sub>2</sub> dimers, which are spectrally active at 4.3  $\mu$ m. Multiphase calculations for atmosphere-ocean systems require knowledge of a surface ocean. In principle, it is possible to infer the presence of exoplanet oceans using ocean glint (Robinson *et al.*, 2010), and the approximate surface extent of oceans may be estimated with time-resolved photometry (Cowan *et al.*, 2009). The sensitivity of our metric to ocean volume is discussed below. Recall also that our multiphase calculations do not fully capture the disequilibrium in the surface reservoirs since they neglect any reactions with the crust (see above).

In principle, the abundances of dissolved ions and ocean pH would also be required to calculate the atmosphere-ocean disequilibrium for an exo-Earth. However, the available Gibbs energy in Earth's atmosphere-ocean system is relatively insensitive to these variables. Table 10 shows the sensitivity of the available Gibbs energy in Earth's atmosphere-ocean system to variables that could not be measured remotely (or would be difficult to observe remotely) on exoplanets. Key findings are summarized below.

The available Gibbs energy of Earth's atmosphere-ocean system is largely insensitive to both ocean salinity and pH. Only at extremely low pH values (pH = 2) does the available energy decrease by around 15% since the equilibrium of Reaction 21 is pushed to the left. This insensitivity arises because the starting abundance of hydrogen ions is many orders of magnitude less than the equilibrium abundance, so changes to the initial abundance (pH) do not affect the equilibrium state very much. This suggests the pH and salinity of exoplanet oceans do not need to be known to estimate the available Gibbs energy in their atmosphere-ocean systems.

The available Gibbs energy of the Earth system is moderately sensitive to ocean volume. Increasing ocean volume by a factor of 10 increases the available Gibbs energy by a factor of 4. The disequilibrium in an exoplanet atmosphere-ocean system could be overestimated if oceans are extremely shallow. For example, if Earth's oceans were only 10% of their current volume, then the available Gibbs en-

TABLE 10. SENSITIVITY OF THE NUMERICAL CALCULATIONS OF THE AVAILABLE GIBBS ENERGY,  $\Phi$ , IN EARTH'S ATMOSPHERE-OCEAN SYSTEM TO PERTURBATIONS IN VARIABLES THAT ARE UNOBSERVABLE OR DIFFICULT TO OBSERVE FOR EXOPLANETS

		Available energy, $\Phi$ (J/mol)
Temperature	$T = 273.15$ K	1634.78
	$T = 288.15$ K	2325.76
	$T = 298.15$ K	2824.48
Pressure	0.1 bar	1354.20
	1.013 bar	2325.76
	10 bar	3891.96
	1000 bar	6878.35
Ocean pH	2	1983.28
	4	2314.26
	6	2325.71
	8.187 (Earth)	2325.76
	12	2325.65
Salinity	0 mol/kg	2290.01
	1.1 mol/kg	2325.76
	11.1 mol/kg	2276.40
Ocean volume	0.1 Earth ocean	413.62
	0.5 Earth ocean	1442.95
	1 Earth ocean	2325.76
	2 Earth oceans	4188.27
	10 Earth oceans	8956.34
	50 Earth oceans	12626.22

ergy in the Earth system would be 413 J/mol, only  $\sim 3$  times larger than our value calculated for Mars (Table 8).

Various observational techniques have been proposed to detect oceans (Gaidos and Williams, 2004; Robinson *et al.*, 2010; Zuger *et al.*, 2010) and map the ocean-land fraction for terrestrial exoplanets with time-resolved photometry (Cowan *et al.*, 2009; Fujii and Kawahara, 2012; Cowan and Strait, 2013). These studies suggest that a  $\sim 10$  m diameter space telescope should be able to obtain a coarse surface map of an Earth analogue at 10 pc. Given observations of surface ocean fraction, it may be possible to constrain ocean depth from geophysical theory. For example, the typical strength or rock would not support a large topographic elevation between seafloor and land. In the case of granitic continents and a basaltic seafloor, the maximum possible ocean depth with exposed continents is approximately equal to  $11.4 \times g_{\text{Earth}}/g_{\text{planet}}$  km, where  $g_{\text{Earth}}$  is the surface gravity of Earth and  $g_{\text{planet}}$  is the surface gravity of the planet of interest (Cowan and Abbot, 2014). Of course, for planets with no land and very deep oceans ( $\sim 1000$  km), ocean volume could be constrained by mass and radius observations. Putting a lower limit on ocean depth is more challenging, but several possibilities exist. Heat flow from planetary interiors is uneven due to the large spacing of convective cells in a viscous fluid and will therefore inevitably create some topographic relief (Davies, 1998). Consequently, the elevation distributions of the terrestrial Solar System planets all extend over several kilometers (Melosh, 2011, p 42). It may also be possible to put a lower bound on ocean volume using thermal inertia arguments and observed variations in a planet's infrared flux over its orbit (Gaidos and Williams, 2004). By

combining land-ocean maps, thermal inertia observations, and geophysical constraints on topography, estimates of ocean volume may be obtainable for some exoplanets, but solving this problem is beyond the scope of the current paper.

Our equilibrium calculation for the Earth atmosphere-ocean system is a simplification because we have assumed the entire atmosphere and ocean are at a mean global temperature and sea-level pressure ( $T=15^\circ\text{C}$  and  $P=1.013$  bar). In practice, the air temperature varies over the surface, ocean temperature typically decreases with depth, and pressure increases by several orders of magnitude in the deep ocean. To investigate the sensitivity of the available Gibbs energy to these variations, we repeated the equilibrium calculation for a wide range of pressures and temperatures. The available Gibbs energy of Earth's atmosphere-ocean system is moderately sensitive to these changes (Table 10). At  $0^\circ\text{C}$  the available Gibbs energy is around 30% lower than the value at the observed mean surface temperature,  $15^\circ\text{C}$ . If temperature is instead increased to  $25^\circ\text{C}$ , then the available Gibbs energy increases by around 20%. Changing the pressure by an order of magnitude in either direction results in a change in available Gibbs energy by approximately a factor of two, though at very high pressures (1000 bar) the available Gibbs energy asymptotes to a value of nearly 7000 J/mol. These results demonstrate that the available Gibbs energy of the Earth atmosphere-ocean system may be somewhat different if spatial variations in temperature and pressure are accounted for, but they also demonstrate that our result ( $\sim 2300$  J/mol) is accurate to well within an order of magnitude. This sensitivity analysis also establishes that it is not necessary to determine the surface temperature and pressure of exoplanets with high precision to estimate the available Gibbs energy of their atmosphere-ocean systems.

In summary, sensitivity analysis suggests that with good observations it might be possible to calculate thermodynamic disequilibrium for exoplanets. The gas phase calculations have no strong sensitivities to difficult-to-observe variables such as ocean volume, so thermodynamic disequilibrium could be accurately calculated from remote observations. Additionally, gas phase reactions are much more weakly dependent on pressure and temperature than multiphase reactions. For multiphase calculations, it may be possible to estimate thermodynamic disequilibrium to the correct order of magnitude. An important caveat on this result is that the available Gibbs energy of Earth is moderately sensitive to ocean volume, and it may be challenging to put a lower bound on ocean depth.

Future work will assess the sensitivity of our metric to potential uncertainties in the inferences from future telescopic observations, which are expected because of limitations such as spectroscopic resolution. Such work is beyond the scope of the current paper, the purpose of which is to describe our basic methodology and discuss results for Solar System bodies.

## 5. Conclusions

- We have quantified the atmospheric chemical disequilibrium for Solar System planets with thick atmospheres. The magnitude of the purely gas phase disequilibrium in Earth's atmosphere, 1.5 J/mol, is not unusual by Solar System standards.

- However, a multiphase equilibrium calculation reveals that the disequilibrium in Earth's atmosphere-ocean system, 2326 J/mol, is at least an order of magnitude larger than any other atmosphere in the Solar System. Note that we did not do a full multiphase calculation for Titan because the mean composition of all its hydrocarbon lakes is not known, so we are comparing the Gibbs energy of Earth's atmosphere-ocean system to other Solar System atmospheres only.
- Earth's disequilibrium is not mainly caused by  $\text{O}_2\text{-CH}_4$  pairing (a contribution of only 1.3 J/mol) but rather by the disequilibrium between  $\text{N}_2\text{-O}_2\text{-H}_2\text{O(l)}$ . This disequilibrium is maintained by life. Oxygenic photosynthesis replenishes molecular oxygen, and the oxidation of fixed nitrogen and biological denitrification prevents the accumulation of nitrate in the ocean.
- The atmospheric composition of terrestrial exoplanets will be accessible to future telescopes, so gas phase thermodynamic disequilibrium may be readily calculated for these planets' atmospheres. It may also be possible to estimate the multiphase disequilibrium for exoplanets if surface oceans can be detected and volumetrically constrained.
- Further work will be required to evaluate the utility of thermodynamic disequilibrium as a generalized metric for surface biospheres.

## Appendix A. Gas Phase Gibbs Minimization

This section describes the methodology used to find gas phase equilibrium by Gibbs free energy minimization. We provide the Matlab code that implements this methodology on the Web site of the senior author (D.C.C.). Recall that, for a gas phase system, the equilibrium state has mole fraction abundances,  $\bar{n}_i$ , that minimize Eq. 5 in the main text. Temperature-dependent standard Gibbs free energies of formation,  $\Delta_f G_{i(T,P_r)}^\circ$ , were calculated from enthalpies and entropies of formation retrieved from NASA's thermodynamic database (Burcat and Ruscic, 2005). We used the 2009 version of this database (available at <http://www.grc.nasa.gov/www/CEAWeb> or <http://garfield.chem.elte.hu/Burcat/NEWNASA.TXT>). The database provides 10 coefficients for each gaseous species (sometimes multiple sets of 10 coefficients are specified for different temperature ranges). The enthalpies and entropies of formation are calculated from these coefficients using the following empirically fitted expressions:

$$\begin{aligned} \Delta_f H_{i(T,P_r)}^\circ / RT = & -a_1 T^{-2} + a_2 \ln(T)/T + a_3 + a_4 T/2 \\ & + a_5 T^2/3 + a_6 T^3/4 + a_7 T^4/5 + a_9/T \end{aligned} \quad (24)$$

$$\begin{aligned} \Delta_f S_{i(T,P_r)}^\circ / R = & -a_1 T^{-2}/2 - a_2/T + a_3 \ln(T) + a_4 T \\ & + a_5 T^2/2 + a_6 T^3/3 + a_7 T^4/4 + a_{10} \end{aligned} \quad (25)$$

Here,  $a_{1-10}$  are the coefficients from the NASA database (the 8<sup>th</sup> coefficient is unused). Enthalpies and entropies are combined to calculate the Gibbs free energy of formation:

$$\Delta_f G_{i(T,P_r)}^\circ = \Delta_f H_{i(T,P_r)}^\circ - T \Delta_f S_{i(T,P_r)}^\circ \quad (26)$$

Note that there are several different conventions for Gibbs free energies of formation (see for instance Anderson and

Crerar, 1993, p 154). The different conventions produce equivalent equilibrium results, but it is important to use Gibbs energies of the same convention within any given calculation. The NASA database provides Gibbs free energies of formation according to the Berman-Brown convention (*e.g.*, Anderson and Crerar, 1993, p 156), but we convert these to standard free energies of formation in our Matlab code.

In the expression for Gibbs energy, Eq. 5, temperature-dependent fugacity coefficients,  $\gamma_{fi}$ , were calculated using the Soave equation as described in Walas (1985, p 146):

$$\ln(\gamma_f) = \frac{B_i}{B}(Z-1) - \ln(Z-B) + \frac{A}{B} \left[ \frac{B_i}{B} - \frac{2}{a\alpha} \sum_j n_j(\alpha\alpha)_{ij} \right] \ln \left( 1 + \frac{B}{Z} \right) \quad (27)$$

Here,  $Z$  is the smallest real solution to the cubic,  $f(Z) = Z^3 - Z^2 + (A - B - B^2)Z - AB = 0$ . The other terms and variables are defined by the following set of equations:

$$\begin{aligned} A &= (\alpha\alpha)P/R^2T^2 & B &= bP/RT \\ B_i &= b_iP/RT & a\alpha &= \sum_i \sum_j n_i n_j (\alpha\alpha)_{ij} \\ (\alpha\alpha)_{ij} &= (1 - k_{ij}) \sqrt{(a_i \alpha_i)(a_j \alpha_j)} & (28) \\ a_i &= 0.42747 R^2 T_{ci}^2 / P_{ci} \\ b_i &= 0.08664 RT_{ci} / P_{ci} & b &= \sum_i n_i b_i \\ \alpha_i &= [1 + (0.480 + 1.574\omega_i - 0.176\omega_i^2)(1 - T_{ci}^{0.5})]^2 \end{aligned}$$

In this set of equations,  $n_i$  is the number of moles of the  $i^{\text{th}}$  species,  $R$  is the universal gas constant, and  $P$  and  $T$  are the pressure and temperature of the system, respectively.  $T_{ci}$  is the critical temperature of the  $i^{\text{th}}$  species, and  $P_{ci}$  is the critical pressure of the  $i^{\text{th}}$  species. Finally,  $\omega_i$  is the acentric factor of the  $i^{\text{th}}$  species, and  $k_{ij}$  is a binary interaction parameter for species  $i$  and  $j$ . All the other variables and terms are computable from these basic parameters. Critical temperatures, critical pressures, and acentric factors for gaseous species were obtained from the work of Perry and Green (2008, Section 2-136). To investigate the importance of binary interaction parameters, we performed some sensitivity tests using the simple gaseous system described by Lwin (2000). In this system,  $\text{H}_2\text{O}$  and  $\text{CH}_4$  are reacted to equilibrium to form  $\text{CO}$ ,  $\text{CO}_2$ , and  $\text{H}_2$  at high temperature (1000 K) and pressure (90 bar). We performed these tests at high temperature and pressure because this is the regime where departure from ideal behavior is the most significant. The inclusion of binary interaction parameters had a small effect on the fugacity coefficients and a negligible effect (<1%) on the overall change in Gibbs energy of the system. Consequently, in the equations above we assumed  $k_{ij}=0$  for every pair of molecules. The close agreement between our numerical Gibbs free energy calculations, which do not include binary interaction parameters, and the Aspen Plus calculations, which do include binary interaction parameters, is further confirmation that ignoring binary interaction parameters is justified.

Given the Gibbs energies of formation and fugacity coefficients for all species, the Gibbs energy expression, Eq. 5, can be computed and minimized. We used an interior points method implemented using Matlab's *fmincon* function to minimize

$\Delta G_{(T,P)}$ . The  $n_i$  that minimize  $\Delta G_{(T,P)}$  and satisfy the atom conservation constraint (Eq. 6) define the equilibrium state.

## Appendix B. Gibbs Energy Proof

Here, we demonstrate that the minimum of Eq. 4 is identical to the minimum of Eq. 5. The standard Gibbs free energy of formation for a compound is the change in Gibbs energy with formation of 1 mol from its constituent elements in their standard states [*i.e.*, the most stable elemental form at standard conditions, usually taken as 25°C and 1 atm for most databases (Anderson and Crerar, 1993, p 154; Anderson, 2005, p 211)]:

$$\Delta_f G_{i(T,P_r)}^\circ \equiv G_{i(T,P_r)}^\circ - \sum_{\text{elements}=j} v_{ji} G_{j(T,P_r)}^\circ \quad (29)$$

Recall that  $v_{ji}$  is the number of atoms of element  $j$  per molecule of species  $i$ , and  $G_{j(T,P_r)}^\circ$  is the standard partial molar Gibbs free energy of gas  $j$  at reference pressure  $P_r$  and temperature  $T$ . The other variables are defined in the main text. Equation 29 can be substituted into Eq. 5 to obtain the following expression:

$$\begin{aligned} \Delta G_{(T,P)} &= \sum_i n_i (\Delta_f G_{i(T,P_r)}^\circ + RT \ln(P_i \gamma_{fi})) \\ &= \sum_i n_i (G_{i(T,P_r)}^\circ - \sum_{\text{elements}=j} v_{ji} G_{j(T,P_r)}^\circ) \\ &\quad + RT \ln(P n_i \gamma_{fi} / n_r) \\ &= G_{(T,P)} - \sum_i \sum_{\text{elements}=j} n_i v_{ji} G_{j(T,P_r)}^\circ \\ &= G_{(T,P)} - \sum_{\text{elements}=j} G_{j(T,P_r)}^\circ \sum_i n_i v_{ji} \end{aligned} \quad (30)$$

Here we use Eq. 4 to substitute for  $G_{(T,P)}$ .

It is often assumed that  $G_{j(T,P_r)}^\circ = 0$  for the elements, thereby establishing that  $\Delta G_{(T,P)} = G_{(T,P)}$ . However, this assumption is incorrect (Anderson and Crerar, 1993, p 147). Instead, the Gibbs free energy of formation for elements equals zero,  $\Delta_f G_{i(T,P_r)}^\circ = 0$  if species  $i$  is an element. Consequently, Eqs. 4 and 5 are not identical ( $\Delta G_{(T,P)} \neq G_{(T,P)}$ ), but they do have the same minimum. This can be seen by considering the second term on the last line of Eq. 30. Conservation of atoms ensures that this term is a constant; refer to Eq. 6 if this is not immediately clear. Since this term is a constant, minimizing  $G_{(T,P)}$  is equivalent to minimizing  $\Delta G_{(T,P)}$ . Note also that because  $G_{(T,P)}$  and  $\Delta G_{(T,P)}$  only differ by a constant, differences in Gibbs energies between two states will be the same regardless of which form is used. This establishes that using Eq. 7 to calculate our metric of available Gibbs energies is equivalent to using Eq. 8.

## Appendix C. Multiphase Calculations

This section describes the methodology used to find multiphase equilibrium by Gibbs free energy minimization. Recall that for a multiphase system, the equilibrium state is the mole fraction abundances,  $\bar{n}_i$ , that minimize the expression in Eq. 9 in the main text. Temperature and pressure-dependent standard Gibbs free energies of formation were calculated from the SUPCRT database (Johnson *et al.*, 1992). Gibbs free energies of formation for aqueous species are given by the following expression (Walther, 2009, p 704):

$$\begin{aligned}
 \Delta_f G_{i(T,P)}^\circ &= \Delta_f G_{i(T_r,P_r)}^\circ - \Delta_f S_{i(T_r,P_r)}^\circ (T - T_r) \\
 &- C_1 \left[ T \ln \left( \frac{T}{T_r} \right) - T + T_r \right] \\
 &+ a_1 (P - P_r) + a_2 \ln \left( \frac{\Psi + P}{\Psi + P_r} \right) \\
 &- c_2 \left\{ \left[ \left( \frac{1}{T - \theta} \right) - \left( \frac{1}{T_r - \theta} \right) \right] \left( \frac{\theta - T}{\theta} \right) \right. \\
 &\left. - \frac{T}{\theta^2} \ln \left[ \frac{T_r (T - \theta)}{T (T_r - \theta)} \right] \right\} \\
 &+ \left( \frac{1}{T - \theta} \right) \left[ a_3 (P - P_r) + a_4 \ln \left( \frac{\Psi + P}{\Psi + P_r} \right) \right] \\
 &+ \omega_{P,T} \left( \frac{1}{\varepsilon_{P,T}} - 1 \right) - \omega_{P_r,T_r} \left( \frac{1}{\varepsilon_{P_r,T_r}} - 1 \right) \\
 &+ \omega_{P_r,T_r} Y_{P_r,T_r} (T - T_r) \quad (31)
 \end{aligned}$$

where

$\Delta_f G_{i(T,P)}^\circ$  = Gibbs free energy of formation for the  $i^{\text{th}}$  species  
 $\Delta_f G_{i(T_r,P_r)}^\circ$  = Gibbs free energy of formation for the  $i^{\text{th}}$  species at the reference temperature and pressure (from SUPCRT database)

$\Delta_f S_{i(T_r,P_r)}^\circ$  = entropy of formation at the reference temperature and pressure

$T$  = temperature of the system

$T_r$  = reference temperature (298 K)

$P$  = pressure of the system

$P_r$  = reference pressure (1 bar)

$c_1, c_2, a_{1-4}$  = species-specific coefficients (from the SUPCRT database)

$\Psi$  = solvent pressure parameter (2600 bar)

$\theta$  = solvent temperature parameter (228 K)

$\omega_{P,T}$  = Born coefficient

$\omega_{P_r,T_r}$  = Born coefficient at the reference temperature and pressure (from the SUPCRT database)

$\varepsilon_{P,T}$  = dielectric constant of water

$\varepsilon_{P_r,T_r}$  = dielectric constant of water at the reference temperature and pressure (78.47)

$Y_{P_r,T_r}$  = Born derivative equation ( $-5.81 \times 10^{-5} \text{ K}^{-1}$ )

The Born coefficients have a small effect on the overall Gibbs energy of formation. For neutral species,  $\omega_{P_r,T_r} = \omega_{P,T}$ . In other cases, these two terms are nearly equal and will approximately cancel each other. Thus, we simplified the Gibbs energy of formation expression by dropping these two terms:

$$\begin{aligned}
 \Delta_f G_{i(T,P)}^\circ &= \Delta_f G_{i(T_r,P_r)}^\circ - \Delta_f S_{i(T_r,P_r)}^\circ (T - T_r) \\
 &- c_1 \left[ T \ln \left( \frac{T}{T_r} \right) - T + T_r \right] \\
 &+ a_1 (P - P_r) + a_2 \ln \left\{ \frac{\Psi + P}{\Psi + P_r} \right\} \\
 &- c_2 \left\{ \left[ \left( \frac{1}{T - \theta} \right) - \left( \frac{1}{T_r - \theta} \right) \right] \left( \frac{\theta - T}{\theta} \right) \right. \\
 &\left. - \frac{T}{\theta^2} \ln \left[ \frac{T_r (T - \theta)}{T (T_r - \theta)} \right] \right\} \\
 &+ \left( \frac{1}{T - \theta} \right) \left[ a_3 (P - P_r) + a_4 \ln \left( \frac{\Psi + P}{\Psi + P_r} \right) \right] \\
 &+ \omega_{P_r,T_r} Y_{P_r,T_r} (T - T_r) \quad (32)
 \end{aligned}$$

This expression is used to calculate the Gibbs free energies of formation for all the aqueous species in our multiphase equilibrium code.

Activity coefficients for aqueous species,  $\gamma_{ai}$  in Eq. 9, were approximated using the Truesdell-Jones equation (Langmuir, 1997, p 140):

$$\ln(\gamma_{ai}) = \frac{-0.5092z_i^2\sqrt{I}}{1 + 0.3283a_i\sqrt{I}} + b_i I \quad (33)$$

Here,  $I = \frac{1}{2} \sum_j m_j Z_j^2$  is the ionic strength of the solution,

where  $m_j$  is the molality of the  $j^{\text{th}}$  species and  $z_j$  is the charge of the  $j^{\text{th}}$  species. The variables  $a_i$  and  $b_i$  are species-specific thermodynamic coefficients that were obtained from Langmuir (1997). The Truesdell-Jones equation is only an approximation, but it is known to be accurate for solutions up to 2 molal (Langmuir, 1997, p 142). Because Earth's ocean has an ionic strength of 0.7 molal, and the dissolution of nitrate and hydrogen by reaction to equilibrium does not increase this very much (see Table 7), the Truesdell-Jones equation provides accurate activity coefficients in our calculations. Sensitivity analysis also reveals that the available Gibbs free energy of Earth is fairly insensitive to the activity coefficients of the major aqueous species. However, the available Gibbs energy of Earth's atmosphere-ocean system is quite sensitive to water activity. Consequently, rather than use the Truesdell-Jones approximation above, the activity coefficient for water was calculated rigorously using a simplified form of the Pitzer equations (Marion and Kargel, 2007):

$$\phi = 1 + \frac{2}{\sum_i m_i} \left\{ \frac{-0.3915I^{3/2}}{1 + 1.2I^{1/2}} + \sum_{\text{all pairs}} m_c m_a (B_{ca}^\phi + ZC_{ca}) \right\} \quad (34)$$

Here,  $\phi$  is the osmotic coefficient and can be related to the activity coefficient of water,  $\gamma_{aw}$  in Eq. 9, by the following expression:

$$\ln(\gamma_{aw}) = -\phi \sum_i m_i / 55.50844 \quad (35)$$

The double summation in Eq. 34 is over all unique pairs of anions and cations in solution (no double counting). The other variables in Eq. 34 are defined as follows:

$m_i$  = molality of the  $i^{\text{th}}$  species

$m_a$  = molality of the anion

$m_c$  = molality of the cation

$I$  = ionic strength of the solution (defined above)

$Z = \sum_i m_i |z_i|$

$B_{MX} = B_{MX}^{(0)} + B_{MX}^{(1)} \exp(-\alpha_1 I^{1/2}) + B_{MX}^{(2)} \exp(-\alpha_2 I^{1/2})$

$\alpha_1 = 2.0 \text{ kg}^{0.5} \text{ mol}^{-0.5}$ ,  $\alpha_2 = 0 \text{ kg}^{0.5} \text{ mol}^{-0.5}$  for all binary systems except 2:2 electrolytes

$\alpha_1 = 1.4 \text{ kg}^{0.5} \text{ mol}^{-0.5}$ ,  $\alpha_2 = 12 \text{ kg}^{0.5} \text{ mol}^{-0.5}$  for 2:2 electrolytes

$B_{MX}^{(0)}, B_{MX}^{(1)}, B_{MX}^{(2)}, C_{MX}$  are species-specific binary interaction parameters that were obtained from the work of Appelo and Postma (2005) and Marion (2002). The form of the Pitzer equation described above is a simplification of the complete

expression; we have ignored cation-cation and anion-anion interactions, neutral solute parameters, and triple particle parameters since these terms will be small for Earth's ocean. Temperature dependencies were also ignored since, in absolute kelvin, the temperature of the ocean is close to the reference temperature of 298 K. The activity coefficient of water was calculated by using these equations at every iteration in our multiphase Gibbs free energy minimization calculations.

Finding the equilibrium state for multiphase systems is more challenging than for single-phase gaseous systems. The Matlab function *fmincon* was once again used to implement the optimization, but this time we provided the analytic gradient for the Gibbs energy function in Eq. 9 from differentiation, as follows:

$$\frac{1}{RT} \frac{\partial \Delta G(T, P)}{\partial n_i} = \left\{ \begin{array}{l} \frac{\Delta_f G_{i(T, P)}^\circ}{RT} + \ln(\gamma_{aw}) + \ln\left(\frac{n_i}{n_{aq}}\right) \\ - \frac{n_i}{n_{aq}} - \frac{n_{aq}}{n_i} + 2 \quad \alpha = \text{water} \\ \frac{\Delta_f G_{i(T, P)}^\circ}{RT} + \ln\left(\frac{n_i}{n_\alpha}\right) + \ln(\gamma_{fi}) \quad \alpha = \text{gas} \\ \frac{\Delta_f G_{i(T, P)}^\circ}{RT} + \ln(55.5084) + \ln(\gamma_{ai}) \\ + \ln\left(\frac{n_i}{n_{aq}}\right) - \ln\left(\frac{n_w}{n_{aq}}\right) - \frac{n_w}{n_{aq}} + 1 \quad \alpha = \text{aqueous} \end{array} \right. \quad (36)$$

The terms in this expression are defined in the methods section. We assumed that the activity coefficients were, to first order, independent of molar abundances.

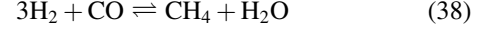
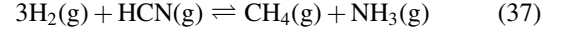
Providing *fmincon* with an analytic gradient ensured more rapid and reliable convergence. For multiphase Gibbs energy minimization problems, there is no guarantee that the local minima equal the global minimum (Nichita *et al.*, 2002). Consequently, we implemented a simple global minimum search by iterating over an ensemble of random initial conditions. The vast majority of runs converged to the same minimum; only occasionally would an optimization run converge to another, less optimum, minimum or simply not converge. This gives us confidence that the consensus minimum was in fact the true global minimum. Semi-analytic calculations and Aspen Plus results also validate our multiphase Gibbs energy minimization result.

#### Appendix D. Semianalytic Calculations

Here, we describe the methodology for our semianalytic calculation using equilibrium reactions in the atmospheres of Jupiter and Earth as examples. The reactions chosen for the semianalytic calculations for the other atmospheres are also listed at the end.

##### Jupiter

In Jupiter's atmosphere, the key available redox couples suggest that there are two important reactions that contribute to chemical disequilibrium:



We begin with Reaction 37. The Gibbs energy of this reaction is given by (*e.g.*, Anderson and Crerar, 1993, p 238)

$$\Delta_r G = \Delta_r G^\circ + RT \ln(Q) = \Delta_r G^\circ + RT \ln\left(\frac{a_{\text{CH}_4} a_{\text{NH}_3}}{a_{\text{H}_2}^3 a_{\text{HCN}}}\right) \quad (39)$$

The activity of each species  $i$  is denoted by  $a_i$ , the temperature of Jupiter's atmosphere at 1 bar is  $T = 165$  K,  $R$  is the universal gas constant, and  $Q$  is the reaction quotient. From Eq. 37 the Gibbs energy of the reaction,  $\Delta_r G$ , is the change in Gibbs energy of the system per 3 mol of  $\text{H}_2$  and 1 mol of  $\text{HCN}$  that are converted to  $\text{CH}_4$  and  $\text{NH}_3$ . The standard free energy of the reaction,  $\Delta_r G^\circ$ , represents the value of this quantity when the activities of all species equal unity. In this case, taking  $T = 165$  K and  $P_r = 1$  bar,

$$\begin{aligned} \Delta_r G^\circ &= \Delta_f G_{\text{CH}_4(T, P_r)}^\circ + \Delta_f G_{\text{NH}_3(T, P_r)}^\circ - 3\Delta_f G_{\text{H}_2(T, P_r)}^\circ \\ &\quad - \Delta_f G_{\text{HCN}(T, P_r)}^\circ \\ &= -6.025 \times 10^4 + -2.88021 \times 10^4 \\ &\quad - 3 \times 0 - 1.27374866 \times 10^5 \text{ J/mol} \\ &= -2.1643 \times 10^5 \text{ J/mol} \end{aligned} \quad (40)$$

where we have substituted the appropriate Gibbs free energies of formation for each species computed at 165 K using the database and methodology of Appendix A. Gibbs free energies of formation were taken from the same thermodynamic databases as those used for the Gibbs energy minimization calculations.

Reaction 37 is in equilibrium when the left-hand side of Eq. 39 is zero. We solve for this equilibrium by making the following substitution:

$$\Delta_r G(x) = \Delta_r G^\circ + RT \ln\left(\frac{[P(n_{\text{CH}_4} + x)/n_T][P(n_{\text{NH}_3} + x)/n_T]}{[P(n_{\text{H}_2} - 3x)/n_T]^3 [P(n_{\text{HCN}} - x)/n_T]}\right) \quad (41)$$

Here,  $n_i$  is the observed moles for each species,  $n_T$  is the total number of moles,  $P$  is the pressure, and  $x$  is the number of moles that have reacted. We solve for  $x$  to find the equilibrium abundances for each species. Note that since we are performing this calculation at  $P = 1$  bar in Jupiter's atmosphere, and since we are using mixing ratios for the number of moles ( $n_T = 1$ ), Eq. 41 can be simplified:

$$\Delta_r G(x) = \Delta_r G^\circ + RT \ln\left(\frac{(n_{\text{CH}_4} + x)(n_{\text{NH}_3} + x)}{(n_{\text{H}_2} - 3x)^3 (n_{\text{HCN}} - x)}\right) \quad (42)$$

By setting  $\Delta_r G(x) = 0$ , this equation can be rearranged to give the following polynomial:

$$\begin{aligned} (n_{\text{H}_2} - 3x)^3 (n_{\text{HCN}} - x) \exp\left(-\frac{\Delta_r G^\circ}{RT}\right) \\ - (n_{\text{CH}_4} + x)(n_{\text{NH}_3} + x) = 0 \end{aligned} \quad (43)$$

This polynomial in  $x$  is solved numerically. The equilibrium is the smallest real solution since the reaction will proceed to this point. In this case this solution is  $x_{\text{eqm}} = 3.6 \times 10^{-9}$ . This solution equals the initial mixing ratio of HCN (Table 3), which implies that Reaction 37 goes to completion when Jupiter's atmosphere is reacted to equilibrium.

To calculate the change in Gibbs energy change associated with this reaction going to completion, we calculate the integral:

$$\begin{aligned} \int_{x=0}^{x=3.6 \times 10^{-9}} \Delta_r G(x')/n_T dx' &= \int_{x=0}^{x=3.6 \times 10^{-9}} \Delta_r G(x') dx' \\ &= \int_{x=0}^{x=3.6 \times 10^{-9}} \left[ \Delta_r G^\circ + RT \ln \left( \frac{(n_{\text{CH}_4} + x')(n_{\text{NH}_3} + x')}{(n_{\text{H}_2} - 3x')^3 (n_{\text{HCN}} - x')} \right) \right] dx' \\ &= 7.5137 \times 10^{-4} \text{ J/mol} \end{aligned} \quad (44)$$

The same methodology can be repeated for Reaction 38.

$$\Delta_r G = \Delta_r G^\circ + RT \ln(Q) = \Delta_r G^\circ + RT \ln \left( \frac{a_{\text{CH}_4} a_{\text{H}_2\text{O}}}{a_{\text{H}_2}^3 a_{\text{CO}}} \right) \quad (45)$$

In this case, the standard free energy of the reaction computed at  $T=165$  K is  $\Delta_r G^\circ = -1.68862 \times 10^5$  J/mol. Substituting activities for  $x$  and simplifying yields the equation:

$$\Delta_r G(x) = \Delta_r G^\circ + RT \ln \left( \frac{(n_{\text{CH}_4} + x)(n_{\text{H}_2\text{O}} + x)}{(n_{\text{H}_2} - 3x)^3 (n_{\text{CO}} - x)} \right) \quad (46)$$

Next, the Gibbs energy of the reaction is set to zero, and terms are rearranged to obtain the polynomial:

$$(n_{\text{H}_2} - 3x)^3 (n_{\text{CO}} - x) \exp \left( -\frac{\Delta_r G^\circ}{RT} \right) - (n_{\text{CH}_4} + x)(n_{\text{H}_2\text{O}} + x) = 0 \quad (47)$$

The solution to this polynomial is  $x_{\text{eqm}} = 1.6 \times 10^{-9}$ , which indicates that CO is depleted and this reaction also goes to completion. The change in Gibbs free energy associated with this reaction is given by

$$\int_{x=0}^{x=1.6 \times 10^{-9}} \Delta_r G(x) dx = 2.8068 \times 10^{-4} \text{ J/mol} \quad (48)$$

Finally, we sum together the Gibbs energy changes from these two reactions to obtain an approximation of the available Gibbs energy in Jupiter's atmosphere:

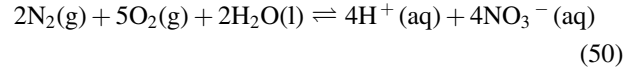
$$\Phi \approx 7.5137 \times 10^{-4} + 2.8068 \times 10^{-4} = 0.001032 \text{ J/mol} \quad (49)$$

This compares to 0.001032 J/mol using the numerical model (main text, Table 3), so the semianalytic approximation is good to four significant figures in this instance.

#### Earth (atmosphere-ocean)

Next, we describe our semianalytic calculations for the Earth atmosphere-ocean system. These calculations were

used to obtain the ‘‘semianalytic approximation’’ values in Tables 8 and 9. Firstly, we consider the Gibbs energy associated with the equation:



The Gibbs energy of this reaction is given by

$$\Delta_r G = \Delta_r G^\circ + RT \ln(Q) = \Delta_r G^\circ + RT \ln \left( \frac{a_{\text{H}^+}^4 a_{\text{NO}_3^-}^4}{a_{\text{N}_2}^2 a_{\text{O}_2}^5 a_{\text{H}_2\text{O}}^2} \right) \quad (51)$$

The activity of each species  $i$  is denoted by  $a_i$ , the average temperature of Earth's atmosphere at the surface is  $T=288.15$  K,  $R$  is the universal gas constant, and  $Q$  is the reaction quotient. From Eq. 50 the Gibbs energy of the reaction,  $\Delta_r G$ , is the change in Gibbs energy of the system per 2 mol of  $\text{N}_2$ , 5 mol of  $\text{O}_2$ , and 2 mol of  $\text{H}_2\text{O}(\text{l})$  that are converted to hydrogen ions and nitrate. The standard free energy of the reaction,  $\Delta_r G^\circ$ , represents the value of this quantity when the activities of all species equal unity. In this case, with  $T=288.15$  K and  $P=P_r=1$  bar:

$$\begin{aligned} \Delta_r G^\circ &= 4\Delta_f G_{\text{H}^+}^\circ(T, P) + 4\Delta_f G_{\text{NO}_3^-}^\circ(T, P) - 2\Delta_f G_{\text{H}_2\text{O}(\text{l})}^\circ(T, P) \\ &\quad - 5\Delta_f G_{\text{O}_2}^\circ(T, P) - 2\Delta_f G_{\text{N}_2}^\circ(T, P) \\ &= 4 \times 0 + 4 \times -1.09164 \times 10^5 - 2 \\ &\quad \times -2.387764 \times 10^5 - 5 \times 0 - 2 \times 0 \text{ J/mol} \\ &= 4.0897 \times 10^4 \text{ J/mol} \end{aligned} \quad (52)$$

Gibbs free energies of formation were taken from the same thermodynamic databases as those used for the Gibbs energy minimization calculations. Reaction 50 is in equilibrium when the left-hand side of Eq. 51 is equal to zero. We solve for this equilibrium by making the following substitution:

$$\Delta_r G(x) = \Delta_r G^\circ + RT \ln \left( \frac{[\gamma_{\text{H}^+} (n_{\text{H}^+} + 4x)/M_{\text{ocean}}]^4 [\gamma_{\text{NO}_3^-} (n_{\text{NO}_3^-} + 4x)/M_{\text{ocean}}]^4}{[P(n_{\text{N}_2} - 2x)/n_T]^2 [P(n_{\text{O}_2} - 5x)/n_T]^5 a_{\text{H}_2\text{O}}^2} \right) \quad (53)$$

The activities of aqueous species are given by their molalities multiplied by an activity coefficient. Here,  $M_{\text{ocean}} = 1.3802 \times 10^{21}$  kg is the mass of Earth's ocean,  $n_i$  is the observed moles for each species,  $n_T = 1.7560 \times 10^{20}$  is the total number of moles of air (all gases) in the atmosphere,  $P = 1.013$  bar is the mean sea-level pressure, and  $x$  is the number of moles that have reacted. We solve for  $x$  to find the equilibrium abundances for each species. By setting the left-hand side of Eq. 53 to zero, assuming that the activity of water equals 1, and that the activity coefficients of all other species are 1, we obtain the following polynomial in  $x$ :

$$\begin{aligned} & \left(\frac{P}{n_T}\right)^7 (n_{N_2} - 2x)^2 (n_{O_2} - 5x)^5 e^{-\frac{\Delta_r G^\circ}{RT}} \\ & = \left(\frac{1}{M_{ocean}^8}\right) (n_{H^+} + 4x)^4 (n_{NO_3} + 4x)^4 \end{aligned} \quad (54)$$

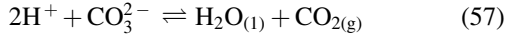
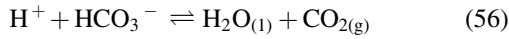
This polynomial is solved numerically. The equilibrium is the smallest real solution since the reaction will proceed to this point. In this case, this solution is  $x_{eqm} = 6.05586 \times 10^{18}$ . This solution does not equal the initial mixing ratio of  $O_2$ , which implies that reaction does not go all the way to completion.

To calculate the change in Gibbs energy change associated with Reaction 50 going to equilibrium, we calculate the integral:

$$\Delta G_1 = \int_{x=0}^{x=6.055 \times 10^{18}} \Delta_r G(x)/n_T dx = 1051 \text{ J/mol} \quad (55)$$

This is how the ‘‘semianalytic approximation’’ value in row 1, Table 9 was calculated.

Next, we consider the Gibbs energy changes associated with the following carbon-bearing reactions:



The Gibbs energy of Reaction 56, the first dissociation of carbonic acid, is given by

$$\Delta_r G = \Delta_r G^\circ + RT \ln(Q) = \Delta_r G^\circ + RT \ln\left(\frac{a_{H_2O_{(l)}} a_{CO_{2(g)}}}{a_{H^+} a_{HCO_3^-}}\right) \quad (58)$$

The method for calculating the Gibbs energy change for this reaction is identical to that described above, so we simply list the key equations:

$$\begin{aligned} \Delta_r G^\circ & = \Delta_f G^\circ_{H_2O_{(l)}(T, P_r)} + \Delta_f G^\circ_{CO_{2(g)}(T, P_r)} \\ & \quad - \Delta_f G^\circ_{H^+(T, P)} - 5\Delta_f G^\circ_{HCO_3^-(T, P)} \\ & = 4.7475 \times 10^4 \text{ J/mol, with} \\ & T = 288 \text{ K and } P = P_r = 1 \text{ bar} \end{aligned} \quad (59)$$

$$\begin{aligned} 0 & = \Delta_r G(x) = \Delta_r G^\circ \\ & + RT \ln\left(\frac{[P(n_{CO_2} + x)/n_T] a_{H_2O}}{[\gamma_{H^+} (n_{H^+} - x)/M_{ocean}] [\gamma_{HCO_3^-} (n_{HCO_3^-} - x)/M_{ocean}]}\right) \end{aligned} \quad (60)$$

Crucially,  $n_{H^+}$  is not the observed  $H^+$  abundance but is instead the equilibrium abundance from Reaction 50; it is the acidification of the ocean from dissolved nitrate that drives the change in carbon species (see main text). Simplifying to obtain polynomial in  $x$ :

$$\begin{aligned} & (n_{H^+} - x) (n_{HCO_3^-} - x) \exp\left(\frac{-\Delta_r G^\circ}{RT}\right) \\ & = M_{ocean}^2 P(n_{CO_2} + x)/n_T \end{aligned} \quad (61)$$

The physically relevant solution is  $x_{eqm} = 2.3951 \times 10^{18}$ . The Gibbs energy change for the reaction can thus be calculated:

$$\Delta G_2 = \int_{x=0}^{x=2.44 \times 10^{18}} \Delta_r G(x)/n_T dx = 520 \text{ J/mol} \quad (62)$$

Repeating this procedure for Eq. 57, the second dissociation of carbonic acid, yields  $\Delta G_3 = 152 \text{ J/mol}$ . The contributions from all three reactions can be summed to approximate the total available Gibbs energy for the Earth atmosphere-ocean system (assuming water activity equals 1):

$$\Phi \approx \Delta G_1 + \Delta G_2 + \Delta G_3 = 1724 \text{ J/mol} \quad (63)$$

This is how the value for the ‘‘semianalytic approximation’’ in Tables 8 and 9 was calculated. There is no straightforward way to extend this semianalytic method to include changes in water activity and, hence, the discrepancy between semianalytic and numerical values.

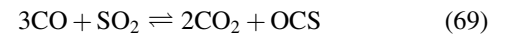
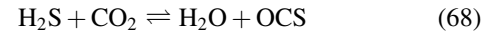
This procedure was repeated to approximate the available Gibbs energy for the Solar System planets. The key redox reactions chosen for these calculations are as follows:

#### Mars



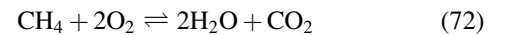
In Mars’ case, all these reactions go to completion.

#### Venus



In Venus’ case, Reactions 70 and 71 go to completion, whereas Reactions 68 and 69 reach equilibria where the reactants are not entirely depleted.

#### Earth (atmosphere only)



All these reactions proceed to completion in Earth’s case.

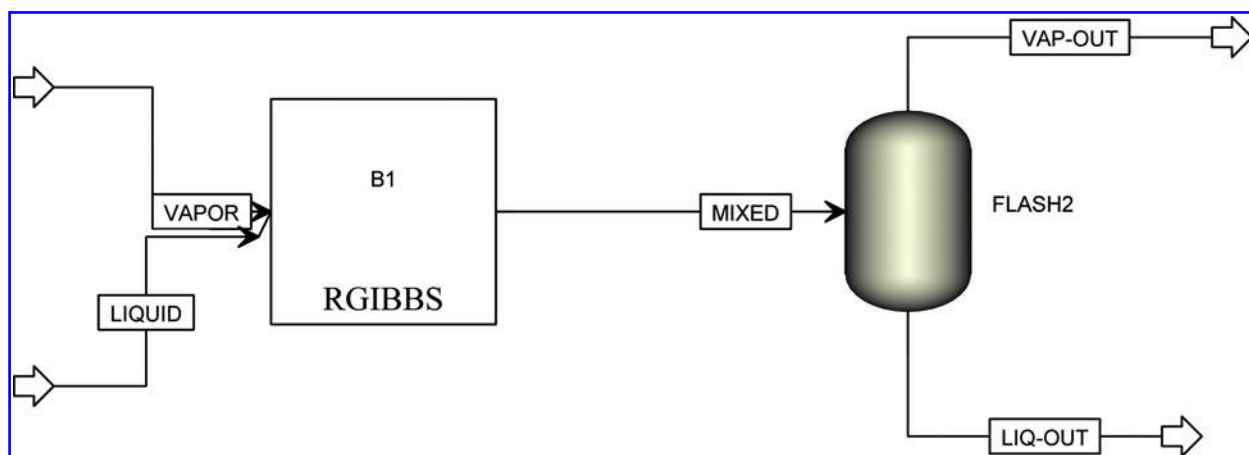
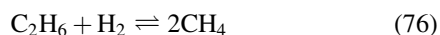


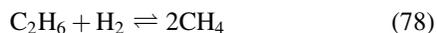
FIG. E1. Aspen Plus flowsheet for multiphase calculations.

#### Titan



Both of these reactions proceed to completion.

#### Uranus



All three reactions proceed to completion.

### Appendix E. Multiphase Calculations in Aspen Plus

To validate our multiphase Matlab calculations, we used Aspen Plus to calculate chemical and phase equilibrium for the Earth atmosphere-ocean system. Figure E1 shows the Aspen Plus flowsheet. The observed state was partitioned into vapor and liquid phases and fed into the RGIBBS reactor as two separate streams. RGIBBS is a module in Aspen Plus that can calculate equilibrium abundances using Gibbs free energy minimization. The resultant mixed stream was fed into a Flash2 phase separator and partitioned into equilibrium vapor abundances and liquid abundances. Without the phase separator the equilibrium results were unphysical, and the resultant Gibbs energy change was inaccurate. We used a calculator block to determine the Gibbs energy change between the two input streams and two output streams. Calculator blocks were necessary to compute the Gibbs energy of the initial and equilibrium states with sufficient precision to calculate the Gibbs energy change accurately (otherwise the default output did not provide enough significant figures).

To check that our results were robust, we used the setup of Fig. E1 to calculate the equilibrium state using two different Aspen Plus electrolyte models, the Electrolyte Non-Random Two Liquid (ELECNRTL) model and the PITZER

model. Henry's law components were used for all gaseous species except water. The equilibrium abundances from both models were very similar. The overall Gibbs energy change of the Earth atmosphere-ocean system was 2348 J/mol for the ELECNRTL model and 2205 J/mol for the PITZER model. It is unsurprising that there are slight differences between the two models since they use different equations of state and different thermodynamic property models. Both agree with our own numerical Gibbs energy minimization to within 6%.

### Acknowledgments

We thank Jonathan D. Toner for assistance with aqueous thermodynamics and implementing the Pitzer equations. We also thank Kathryn Cogert for assistance with Aspen Plus, and the two anonymous reviewers, whose comments greatly improved the clarity and science content of this manuscript. D.C.C. thanks Chris Glein for some assistance on preliminary work at the inception of this project in 2005. This work was supported by Exobiology Program grant NNX10AQ90G awarded to D.C.C., NASA Earth and Space Sciences Fellowship NNX15AR63H awarded to J.K.T., and NASA Astrobiology Institute's Virtual Planetary Laboratory under Cooperative Agreement Number NNA13AA93A. D.S.B. was also supported by the NASA Washington Space Grant when he was an undergraduate researcher with D.C.C. at the University of Washington.

### Disclosure Statement

No competing financial interests exist.

### References

- Anderson, G.M. (2005) *Thermodynamics of Natural Systems*, Cambridge University Press, Cambridge, UK.
- Anderson, G.M. and Crerar, D.A. (1993) *Thermodynamics in Geochemistry: The Equilibrium Model*, Oxford University Press, Oxford, UK.
- Appelo, C.A.J. and Postma, D. (2005) *Geochemistry, Groundwater and Pollution*, CRC Press, Boca Raton, FL.

- Aspen Technology Inc. (2000) *Aspen Plus: Getting Started Modeling Processes with Electrolytes*, Aspen Technology Inc., Cambridge, MA.
- Bada, J.L. and Miller, S.L. (1968) Ammonium ion concentration in the primitive ocean. *Science* 159:423–425.
- Baines, K.H., Atreya, S.K., Bullock, M.A., Grinspoon, D.H., Mahaffy, P., Russell, C.T., Schubert, G., and Zahnle, K. (2014) The atmospheres of the terrestrial planets: clues to the origins and early evolution of Venus, Earth, and Mars. In *Comparative Climatology of Terrestrial Planets*, edited by S.J. Mackwell, A.A. Simon-Miller, J.W. Harder, and M.A. Bullock, University of Arizona Press, Tucson, 137–160.
- Balzhiser, R.E., Samuels, M.R., and Eliassen, J.D. (1972) *Chemical Engineering Thermodynamics: The Study of Energy, Entropy, and Equilibrium*, Prentice-Hall, Englewood Cliffs, NJ.
- Barman, T. (2007) Identification of absorption features in an extrasolar planet atmosphere. *Astrophys J* 661:L191.
- Belu, A., Selsis, F., Morales, J.-C., Ribas, I., Cossou, C., and Rauer, H. (2011) Primary and secondary eclipse spectroscopy with JWST: exploring the exoplanet parameter space. *Astron Astrophys* 525:A83.
- Bézar, B., Lellouch, E., Strobel, D., Maillard, J.-P., and Drossart, P. (2002) Carbon monoxide on Jupiter: evidence for both internal and external sources. *Icarus* 159:95–111.
- Bougher, S.W., Hunten, D.M., and Phillips, R.J. (1997) *Venus II—Geology, Geophysics, Atmosphere, and Solar Wind Environment*, University of Arizona Press, Tucson, AZ.
- Burcat, A. and Ruscic, B. (2005) *Third Millennium Ideal Gas and Condensed Phase Thermochemical Database for Combustion with Updates from Active Thermochemical Tables*, US Department of Energy, Oak Ridge, TN.
- Byrd, R.H., Hribar, M.E., and Nocedal, J. (1999) An interior point algorithm for large-scale nonlinear programming. *SIAM J Optim* 9:877–900.
- Byrd, R.H., Gilbert, J.C., and Nocedal, J. (2000) A trust region method based on interior point techniques for nonlinear programming. *Math Program* 89:149–185.
- Capone, D.G., Popa, R., Flood, B., and Nealson, K.H. (2006) Geochemistry. Follow the nitrogen. *Science* 312:708–709.
- Catling, D. and Bergsman, D. (2009) Using atmospheric composition as a metric for detecting life on habitable planets [abstract #B11E-06]. In *2009 AGU Fall Meeting*, American Geophysical Union, Washington, DC.
- Catling, D. and Bergsman, D. (2010) On detecting exoplanet biospheres from atmospheric chemical disequilibrium [abstract 5533]. In *Astrobiology Science Conference 2010: Evolution and Life: Surviving Catastrophes and Extremes on Earth and Beyond*, Lunar and Planetary Institute, Houston.
- Catling, D. and Kasting, J.F. (2007) Planetary atmospheres and life. In *Planets and Life: The Emerging Science of Astrobiology*, edited by W.T. Sullivan and J.A. Baross, Cambridge University Press, Cambridge, UK, pp 91–116.
- Catling, D.C. (2015) Planetary atmospheres. In *Treatise on Geophysics*, 2<sup>nd</sup> ed., edited by G. Schubert, Elsevier, Amsterdam, pp 429–472.
- Catling, D.C., Zahnle, K.J., and McKay, C.P. (2001) Biogenic methane, hydrogen escape, and the irreversible oxidation of early Earth. *Science* 293:839–843.
- Charbonneau, D., Brown, T.M., Noyes, R.W., and Gilliland, R.L. (2002) Detection of an extrasolar planet atmosphere. *Astrophys J* 568, doi:10.1086/338770.
- Cockell, C.S., Léger, A., Fridlund, M., Herbst, T., Kaltenegger, L., Absil, O., Beichman, C., Benz, W., Blanc, M., and Brack, A. (2009) Darwin—a mission to detect and search for life on extrasolar planets. *Astrobiology* 9:1–22.
- Cordier, D., Mousis, O., Lunine, J.I., Lavvas, P., and Vuitton, V. (2009) An estimate of the chemical composition of Titan's lakes. *Astrophys J* 707:L128.
- Covey, C., Haberle, R.M., McKay, C.P., and Titov, D.V. (2013) The greenhouse effect and climate feedbacks. In *Comparative Climatology of Terrestrial Planets*, edited by S.J. Mackwell, A.A. Simon-Miller, J.W. Harder, and M.A. Bullocks, University of Arizona Press, Tucson, AZ, pp 163–179.
- Cowan, N.B. and Abbot, D.S. (2014) Water cycling between ocean and mantle: super-Earths need not be waterworlds. arXiv:1401.0720
- Cowan, N.B. and Strait, T.E. (2013) Determining reflectance spectra of surfaces and clouds on exoplanets. *Astrophys J* 765:L17.
- Cowan, N.B., Agol, E., Meadows, V.S., Robinson, T., Livengood, T.A., Deming, D., Lisse, C.M., A'Hearn, M.F., Wellnitz, D.D., and Seager, S. (2009) Alien maps of an ocean-bearing world. *Astrophys J* 700, doi:10.1088/0004-637X/700/2/915.
- Davies, G.F. (1998) Topography: a robust constraint on mantle fluxes. *Chem Geol* 145:479–489.
- Deming, D., Seager, S., Winn, J., Miller-Ricci, E., Clampin, M., Lindler, D., Greene, T., Charbonneau, D., Laughlin, G., and Ricker, G. (2009) Discovery and characterization of transiting super Earths using an all-sky transit survey and follow-up by the James Webb Space Telescope. *Publ Astron Soc Pac* 121:952–967.
- Deming, D., Wilkins, A., McCullough, P., Burrows, A., Fortney, J.J., Agol, E., Dobbs-Dixon, I., Madhusudhan, N., Crouzet, N., and Desert, J.-M. (2013) Infrared transmission spectroscopy of the exoplanets HD 209458b and XO-1b using the Wide Field Camera-3 on the Hubble Space Telescope. *Astrophys J* 774, doi:10.1088/0004-637X/774/2/95.
- Des Marais, D.J., Harwit, M.O., Jucks, K.W., Kasting, J.F., Lin, D.N., Lunine, J.I., Schneider, J., Seager, S., Traub, W.A., and Woolf, N.J. (2002) Remote sensing of planetary properties and biosignatures on extrasolar terrestrial planets. *Astrobiology* 2:153–181.
- Devol, A.H. (2008) Nitrogen in the marine environment. In *Nitrogen in the Marine Environment*, edited by D.G. Capone, D.A. Bronk, M.R. Mulholland, and E.J. Carpenters, Academic Press, New York, pp 263–301.
- Dlugokencky, E., Masarie, K., Lang, P., and Tans, P. (1998) Continuing decline in the growth rate of the atmospheric methane burden. *Nature* 393:447–450.
- Eriksson, G. (1971) Thermodynamics studies of high temperature equilibria. 3. SOLGAS, a computer program for calculating composition and heat condition of an equilibrium mixture. *Acta Chem Scand* 25:2651–2658.
- Eriksson, G. (1975) Thermodynamic studies of high-temperature equilibria. 12. SOLGASMIX, a computer program for calculation of equilibrium compositions in multiphase systems. *Chem Scr* 8:100–103.
- Estrada, E. (2012) Returnability as a criterion of disequilibrium in atmospheric reactions networks. *J Math Chem* 50:1363–1372.
- Fegley, B. (2014) Venus. In *Treatise on Geochemistry*, 2<sup>nd</sup> ed., edited by H.D. Holland and K.K. Turekian, Elsevier, Amsterdam, pp 127–148.
- Fraine, J., Deming, D., Benneke, B., Knutson, H., Jordán, A., Espinoza, N., Madhusudhan, N., Wilkins, A., and Todorov, K. (2014) Water vapour absorption in the clear atmosphere of a Neptune-sized exoplanet. *Nature* 513:526–529.

- Fujii, Y. and Kawahara, H. (2012) Mapping Earth analogs from photometric variability: spin-orbit tomography for planets in inclined orbits. *Astrophys J* 755, doi:10.1088/0004-637X/755/2/101.
- Gaidos, E. and Williams, D. (2004) Seasonality on terrestrial extrasolar planets: inferring obliquity and surface conditions from infrared light curves. *New Astronomy* 10:67–77.
- Glein, C.R. and Shock, E.L. (2013) A geochemical model of non-ideal solutions in the methane–ethane–propane–nitrogen–acetylene system on Titan. *Geochim Cosmochim Acta* 115: 217–240.
- Gruber, N. (2008) The marine nitrogen cycle: overview and challenges. In *Nitrogen in the Marine Environment*, edited by D.G. Capone, D.A. Bronk, M.R. Mulholland, and E.J. Carpenters, Academic Press, New York, pp 1–50.
- Hayes, J.M. and Waldbauer, J.R. (2006) The carbon cycle and associated redox processes through time. *Philos Trans R Soc Lond B Biol Sci* 361:931–950.
- Hedelt, P., von Paris, P., Godolt, M., Gebauer, S., Grenfell, J.L., Rauer, H., Schreier, F., Selsis, F., and Trautmann, T. (2013) Spectral features of Earth-like planets and their detectability at different orbital distances around F, G, and K-type stars. *Astron Astrophys* 553:A9.
- Hitchcock, D.R. and Lovelock, J.E. (1967) Life detection by atmospheric analysis. *Icarus* 7:149–159.
- Huguenin, R.L., Prinn, R.G., and Maderazzo, M. (1977) Mars: photodesorption from mineral surfaces and its effects on atmospheric stability. *Icarus* 32:270–298.
- Hutchinson, G. (1954) The biochemistry of the terrestrial atmosphere. In *The Earth as a Planet*, edited by G.P. Kuipers, University of Chicago Press, Chicago, pp 371–433.
- Irwin, P. (2009) *Giant Planets of Our Solar System: Atmospheres, Composition, and Structure*, 2<sup>nd</sup> ed., Springer Science & Business Media, Berlin.
- Jacob, D. (1999) *Introduction to Atmospheric Chemistry*, Princeton University Press, Princeton, NJ.
- Johnson, J.W., Oelkers, E.H., and Helgeson, H.C. (1992) SUPCRT92: a software package for calculating the standard molal thermodynamic properties of minerals, gases, aqueous species, and reactions from 1 to 5000 bar and 0 to 1000 C. *Comput Geosci* 18:899–947.
- Karpov, I.K., Chudnenko, K.V., and Kulik, D.A. (1997) Modeling chemical mass transfer in geochemical processes; thermodynamic relations, conditions of equilibria and numerical algorithms. *Am J Sci* 297:767–806.
- Kasting, J., Traub, W., Roberge, A., Leger, A., Schwartz, A., Wootten, A., Vosteen, A., Lo, A., Brack, A., Tanner, A., Coustenis, A., Lane, B., Oppenheimer, B., Mennesson, B., Lopez, B., Grillmair, C., Beichman, C., Cockell, C., Hanot, C., McCarthy, C., Stark, C., Marois, C., Aime, C., Angerhausen, D., Montes, D., Wilner, D., Defrere, D., Mourard, D., Lin, D., Kite, E., Chassefiere, E., Malbet, F., Tian, F., Westall, F., Illingworth, G., Vasisht, G., Serabyn, G., Marcy, G., Bryden, G., White, G., Laughlin, G., Torres, G., Hammel, H., Ferguson, H., Shibai, H., Rottgering, H., Surdej, J., Wiseman, J., Ge, J., Bally, J., Krist, J., Monnier, J., Trauger, J., Horner, J., Catanzarite, J., Harrington, J., Nishikawa, J., Stapelfeldt, K., von Braun, K., Biazzo, K., Carpenter, K., Balasubramanian, K., Kaltenecker, L., Postman, M., Spaans, M., Turnbull, M., Levine, M., Burchell, M., Ealey, M., Kuchner, M., Marley, M., Dominik, M., Mountain, M., Kenworthy, M., Muterspaugh, M., Shao, M., Zhao, M., Tamura, M., Kasdin, N., Haghighipour, N., Kiang, N., Elias, N., Woolf, N., Mason, N., Absil, O., Guyon, O., Lay, O., Borde, P., Fouque, P., Kalas, P., Lowrance, P., Plavchan, P., Hinz, P., Kervella, P., Chen, P., Akeson, R., Soummer, R., Waters, R., Barry, R., Kendrick, R., Brown, R., Vanderbei, R., Woodruff, R., Danner, R., Allen, R., Polidan, R., Seager, S., MacPhee, S., Hosseini, S., Metchev, S., Kafka, S., Ridgway, S., Rinehart, S., Unwin, S., Shaklan, S., Brummelaar, T. ten, Mazeh, T., Meadows, V., Weiss, W., Danchi, W., Ip, W., and Rabbia, Y. (2009) Exoplanet characterization and the search for life. In *Astro2010: The Astronomy and Astrophysics Decadal Survey*, The National Academies of Sciences, Engineering, and Medicine, Washington, DC.
- Kasting, J.F., Whitmire, D.P., and Reynolds, R.T. (1993) Habitable zones around main sequence stars. *Icarus* 101:108–128.
- Kaye, J.A. and Strobel, D.F. (1983) HCN formation on Jupiter: the coupled photochemistry of ammonia and acetylene. *Icarus* 54:417–433.
- Kirschke, S., Bousquet, P., Ciais, P., Saunois, M., Canadell, J.G., Dlugokencky, E.J., Bergamaschi, P., Bergmann, D., Blake, D.R., and Bruhwiler, L. (2013) Three decades of global methane sources and sinks. *Nat Geosci* 6:813–823.
- Kleidon, A. (2012) How does the Earth system generate and maintain thermodynamic disequilibrium and what does it imply for the future of the planet? *Philos Transact A Math Phys Eng Sci* 370:1012–1040.
- Knutson, H.A., Lewis, N., Fortney, J.J., Burrows, A., Showman, A.P., Cowan, N.B., Agol, E., Aigrain, S., Charbonneau, D., and Deming, D. (2012) 3.6 and 4.5  $\mu\text{m}$  phase curves and evidence for non-equilibrium chemistry in the atmosphere of extrasolar planet HD 189733b. *Astrophys J* 754, doi:10.1088/0004-637X/754/1/22.
- Krasnopolsky, V.A. (2015) Vertical profiles of H<sub>2</sub>O, H<sub>2</sub>SO<sub>4</sub>, and sulfuric acid concentration at 45–75 km on Venus. *Icarus* 252:327–333.
- Krasnopolsky, V.A. and Lefèvre, F. (2013) Chemistry of the atmospheres of Mars, Venus, and Titan. In *Comparative Climatology of Terrestrial Planets*, edited by S.J. Mackwell, A.A. Simon-Miller, J.W. Harder, and M.A. Bullock, University of Arizona Press, Tucson, pp 231–275.
- Langmuir, D. (1997) *Aqueous Environmental Geochemistry*, Prentice Hall, Upper Saddle River, NJ.
- Lederberg, J. (1965) Signs of life. *Nature* 207:9–13.
- Léger, A. (2000) Strategies for remote detection of life—DARWIN-IRSI and TPF missions. *Adv Space Res* 25:2209–2223.
- Lewis, G.N. and Randall, M. (1923) *Thermodynamics and the Free Energy of Chemical Substances*, McGraw-Hill, New York.
- Lewis, J. (2012) *Physics and Chemistry of the Solar System*, Academic Press, Boston.
- Line, M.R. and Yung, Y.L. (2013) A systematic retrieval analysis of secondary eclipse spectra. III. Diagnosing chemical disequilibrium in planetary atmospheres. *Astrophys J* 779, doi:10.1088/0004-637X/779/1/3.
- Lippincott, E.R., Eck, R.V., Dayhoff, M.O., and Sagan, C. (1967) Thermodynamic equilibria in planetary atmospheres. *Astrophys J* 147, doi:10.1086/149051.
- Lodders, K. and Fegley, B. (1998) *The Planetary Scientist's Companion*, Oxford University Press, New York.
- Lorenz, R.D., Kirk, R.L., Hayes, A.G., Anderson, Y.Z., Lunine, J.I., Tokano, T., Turtle, E.P., Malaska, M.J., Soderblom, J.M., and Lucas, A. (2014) A radar map of Titan seas: tidal dissipation and ocean mixing through the throat of Kraken. *Icarus* 237:9–15.
- Lovelock, J.E. (1965) A physical basis for life detection experiments. *Nature* 207:568–570.
- Lovelock, J.E. (1975) Thermodynamics and the recognition of alien biospheres. *Proc R Soc Lond B Biol Sci* 189:167–181.

- Lovelock, J.E. and Margulis, L. (1974) Atmospheric homeostasis by and for the biosphere: the Gaia hypothesis. *Tellus* 26:2–10.
- Lwin, Y. (2000) Chemical equilibrium by Gibbs energy minimization on spreadsheets. *International Journal of Engineering Education* 16:335–339.
- Mahaffy, P.R., Webster, C.R., Atreya, S.K., Franz, H., Wong, M., Conrad, P.G., Harpold, D., Jones, J.J., Leshin, L.A., and Manning, H. (2013) Abundance and isotopic composition of gases in the martian atmosphere from the Curiosity rover. *Science* 341:263–266.
- Marion, G.M. (2002) A molal-based model for strong acid chemistry at low temperatures (<200 to 298 K). *Geochim Cosmochim Acta* 66:2499–2516.
- Marion, G.M. and Kargel, J.S. (2007) *Cold Aqueous Planetary Geochemistry with FREZCHEM: From Modeling to the Search for Life at the Limits*, Springer Science & Business Media, Berlin.
- Melosh, H.J. (2011) *Planetary Surface Processes*, Cambridge University Press, Cambridge, UK.
- Misra, A., Meadows, V., Claire, M., and Crisp, D. (2014) Using dimers to measure biosignatures and atmospheric pressure for terrestrial exoplanets. *Astrobiology* 14:67–86.
- Moses, J.I., Visscher, C., Fortney, J.J., Showman, A.P., Lewis, N.K., Griffith, C.A., Klippenstein, S.J., Shabram, M., Friedson, A.J., and Marley, M.S. (2011) Disequilibrium carbon, oxygen, and nitrogen chemistry in the atmospheres of HD 189733b and HD 209458b. *Astrophys J* 737, doi:10.1088/0004-637X/737/1/15.
- Nair, H., Allen, M., Anbar, A.D., Yung, Y.L., and Clancy, R.T. (1994) A photochemical model of the martian atmosphere. *Icarus* 111:124–150.
- Nichita, D.V., Gomez, S., and Luna, E. (2002) Multiphase equilibria calculation by direct minimization of Gibbs free energy with a global optimization method. *Comput Chem Eng* 26:1703–1724.
- Perry, R.H. and Green, D.W. (2008) *Perry's Chemical Engineers' Handbook*, 8<sup>th</sup> ed., McGraw-Hill, New York.
- Pilson, M.E. (2012) *An Introduction to the Chemistry of the Sea*, Cambridge University Press, Cambridge, UK.
- Pont, F., Knutson, H., Gilliland, R., Moutou, C., and Charbonneau, D. (2008) Detection of atmospheric haze on an extrasolar planet: the 0.55–1.05  $\mu\text{m}$  transmission spectrum of HD 189733b with the Hubble Space Telescope. *Mon Not R Astron Soc* 385:109–118.
- Prausnitz, J.M., Lichtenthaler, R.N., and de Azevedo, E.G. (1999) *Molecular Thermodynamics of Fluid-Phase Equilibria*, Pearson Education, Taiwan.
- Prinn, R., Huang, J., Weiss, R., Cunnold, D., Fraser, P., Simmonds, P., McCulloch, A., Harth, C., Salameh, P., and O'Doherty, S. (2001) Evidence for substantial variations of atmospheric hydroxyl radicals in the past two decades. *Science* 292:1882–1888.
- Prinn, R.G. and Barshay, S.S. (1977) Carbon monoxide on Jupiter and implications for atmospheric convection. *Science* 198:1031–1034.
- Rakov, V.A. and Uman, M.A. (2007) *Lightning: Physics and Effects*, Cambridge University Press, Cambridge, UK.
- Rauer, H., Gebauer, S., Paris, P., Cabrera, J., Godolt, M., Grenfell, J., Belu, A., Selsis, F., Hedelt, P., and Schreier, F. (2011) Potential biosignatures in super-Earth atmospheres: I. Spectral appearance of super-Earths around M dwarfs. *Astron Astrophys* 529, doi:10.1051/0004-6361/201014368.
- Robinson, T.D. and Catling, D.C. (2014) Common 0.1 bar tropopause in thick atmospheres set by pressure-dependent infrared transparency. *Nat Geosci* 7:12–15.
- Robinson, T.D., Meadows, V.S., and Crisp, D. (2010) Detecting oceans on extrasolar planets using the glint effect. *Astrophys J* 721:L67.
- Rodler, F. and López-Morales, M. (2014) Feasibility studies for the detection of O<sub>2</sub> in an Earth-like exoplanet. *Astrophys J* 781, doi:10.1088/0004-637X/781/1/54.
- Sagan, C., Thompson, W.R., Carlson, R., Gurnett, D., and Hord, C. (1993) A search for life on Earth from the Galileo spacecraft. *Nature* 365:715–721.
- Schwartzman, D. and Volk, T. (2004) Does life drive disequilibrium in the biosphere? In *Scientists Debate Gaia: The Next Century*, edited by S.H. Schneider, MIT Press, Cambridge, MA, pp 129–135.
- Schwietzman, E.W., Robinson, T.D., Meadows, V.S., Misra, A., and Domagal-Goldman, S. (2015) Detecting and constraining N<sub>2</sub> abundances in planetary atmospheres using collisional pairs. *Astrophys J* 810, doi:10.1088/0004-637X/810/1/57.
- Seager, S. (2014) The future of spectroscopic life detection on exoplanets. *Proc Natl Acad Sci USA* 111:12634–12640.
- Seager, S. and Bains, W. (2015) The search for signs of life on exoplanets at the interface of chemistry and planetary science. *Sci Adv* 1, doi:10.1126/sciadv.1500047.
- Seager, S. and Deming, D. (2010) Exoplanet atmospheres. *Annu Rev Astron Astrophys* 48:631–672.
- Seager, S., Bains, W., and Hu, R. (2013) A biomass-based model to estimate the plausibility of exoplanet biosignature gases. *Astrophys J* 775, doi:10.1088/0004-637X/775/2/104.
- Sillén, L.G. (1966) Regulation of O<sub>2</sub>, N<sub>2</sub> and CO<sub>2</sub> in the atmosphere; thoughts of a laboratory chemist. *Tellus* 18:198–206.
- Simoncini, E., Virgo, N., and Kleidon, A. (2013) Quantifying drivers of chemical disequilibrium: theory and application to methane in the Earth's atmosphere. *Earth System Dynamics* 4:317–331.
- Sleep, N.H. (2005) Dioxygen over geological time. In *Metal Ions in Biological Systems, Volume 43: Biogeochemical Cycles of Elements*, edited by A. Sigel, H. Sigel, and R.K.O. Sigel, CRC Press, Boca Raton, FL, pp 49–73.
- Smirnov, A., Hausner, D., Laffers, R., Strongin, D.R., and Schoonen, M.A. (2008) Abiotic ammonium formation in the presence of Ni-Fe metals and alloys and its implications for the Hadean nitrogen cycle. *Geochem Trans* 9, doi:10.1186/1467-4866-9-5.
- Snellen, I., de Kok, R., Le Poole, R., Brogi, M., and Birkby, J. (2013) Finding extraterrestrial life using ground-based high-dispersion spectroscopy. *Astrophys J* 764, doi:10.1088/0004-637X/764/2/182.
- Stevenson, K.B., Harrington, J., Nymeyer, S., Madhusudhan, N., Seager, S., Bowman, W.C., Hardy, R.A., Deming, D., Rauscher, E., and Lust, N.B. (2010) Possible thermochemical disequilibrium in the atmosphere of the exoplanet GJ 436b. *Nature* 464:1161–1164.
- Summers, D.P., Basa, R.C., Khare, B., and Rodoni, D. (2012) Abiotic nitrogen fixation on terrestrial planets: reduction of NO to ammonia by FeS. *Astrobiology* 12:107–114.
- Ulanowicz, R.E. and Hannon, B. (1987) Life and the production of entropy. *Proc R Soc Lond B Biol Sci* 232:181–192.
- Venot, O., Hébrard, E., Agúndez, M., Dobrijevic, M., Selsis, F., Hersant, F., Iro, N., and Bounaceur, R. (2013) The nitrogen chemistry in hot Jupiters atmosphere. In *The Early Evolution of the Atmospheres of Terrestrial Planets*, edited by J.M. Trigo-Rodríguez, F. Raulin, C. Muller, and C. Nixon, Springer, New York, pp 67–83.

- Vidal-Madjar, A., Des Etangs, A.L., Désert, J.-M., Ballester, G., Ferlet, R., Hébrard, G., and Mayor, M. (2003) An extended upper atmosphere around the extrasolar planet HD209458b. *Nature* 422:143–146.
- Walas, S.M. (1985) *Phase Equilibria in Chemical Engineering*, Butterworth, Boston, MA.
- Walther, J.V. (2009) *Essentials of Geochemistry*, Jones & Bartlett Publishers, Sudbury, MA.
- Wedepohl, K.H. (1995) The composition of the continental crust. *Geochim Cosmochim Acta* 59:1217–1232.
- White, W.B., Johnson, S.M., and Dantzig, G.B. (1958) Chemical equilibrium in complex mixtures. *J Chem Phys* 28:751–755.
- Younglove, B. and Ely, J.F. (1987) Thermophysical properties of fluids. II. Methane, ethane, propane, isobutane, and normal butane. *J Phys Chem Ref Data* 16:577–798.
- Yung, Y.L. and DeMore, W.B. (1999) *Photochemistry of Planetary Atmospheres*, Oxford University Press, New York.
- Zahnle, K., Haberle, R.M., Catling, D.C., and Kasting, J.F. (2008) Photochemical instability of the ancient martian atmosphere. *J Geophys Res Planets* 113, doi:10.1029/2008JE003160.
- Zhang, X., Liang, M.C., Mills, F.P., Belyaev, D.A., and Yung, Y.L. (2012) Sulfur chemistry in the middle atmosphere of Venus. *Icarus* 217:714–739.
- Zugger, M.E., Kasting, J.F., Williams, D.M., Kane, T.J., and Philbrick, C.R. (2010) Light scattering from exoplanet oceans and atmospheres. *Astrophys J* 723:1168–1179.

Address correspondence to:

Joshua Krissansen-Totton  
Department of Earth and Space Sciences  
Johnson Hall Rm-070  
Box 351310  
4000 15<sup>th</sup> Avenue NE  
University of Washington  
Seattle, WA 98195

E-mail: joshkt@uw.edu

Submitted 26 March 2015

Accepted 5 October 2015